EFFECT OF DIFFERENT IRRADIANCE LEVELS ON BIOELECTRICITY GENERATION FROM ALGAL BIOPHOTOVOLTAIC DEVICES

THONG CHENG HAN

FACULTY OF SCIENCE
UNIVERSITY OF MALAYA
KUALA LUMPUR

2019

EFFECT OF DIFFERENT IRRADIANCE LEVELS ON BIOELECTRICITY GENERATION FROM ALGAL BIOPHOTOVOLTAIC DEVICES

THONG CHENG HAN

DISSERTATION SUBMITTED IN PARTIAL FULFILMENT OF THE REQUIREMENTS FOR THE DEGREE OF MASTER OF TECHNOLOGY (ENVIRONMENTAL MANAGEMENT)

INSTITUTE OF BIOLOGICAL SCIENCES
FACULTY OF SCIENCE
UNIVERSITY OF MALAYA
KUALA LUMPUR

2019

UNIVERSITY OF MALAYA

ORIGINAL LITERARY WORK DECLARATION

Name of Candidate: THONG CHENG HAN

Matric No: SGH 160012

Name of Degree: MASTER OF TECHNOLOGY (ENVIRONMENTAL MANAGEMENT)

Title of Project Paper/Research Report/Dissertation/Thesis ("this Work"):

EFFECT OF DIFFERENT IRRADIANCE LEVELS ON BIOELECTRICITY GENERATION FROM ALGAL BIOPHOTOVOLTAIC DEVICES

Field of Study: ALTERNATIVE ENERGY

I do solemnly and sincerely declare that:

(1) I am the sole author/writer of this Work;
(2) This Work is original;
(3) Any use of any work in which copyright exists was done by way of fair dealing and for permitted purposes and any excerpt or extract from, or reference to or reproduction of any copyright work has been disclosed expressly and sufficiently and the title of the Work and its authorship have been acknowledged in this Work;
(4) I do not have any actual knowledge nor do I ought reasonably to know that the making of this work constitutes an infringement of any copyright work;
(5) I hereby assign all and every rights in the copyright to this Work to the University of Malaya ("UM"), who henceforth shall be owner of the copyright in this Work and that any reproduction or use in any form or by any means whatsoever is prohibited without the written consent of UM having been first had and obtained;
(6) I am fully aware that if in the course of making this Work I have infringed any copyright whether intentionally or otherwise, I may be subject to legal action or any other action as may be determined by UM.

Candidate's Signature   Date:

Subscribed and solemnly declared before,

Witness's Signature   Date:

Name:

Designation:

EFFECT OF DIFFERENT IRRADIANCE LEVELS ON BIOELECTRICITY GENERATION FROM ALGAL BIOPHOTOVOLTAIC DEVICES

ABSTRACT

Photosynthesizing organisms including microalgae are exposed to varying levels of light irradiance throughout the day, thus sparking strong research interests in determining the effects of different irradiance levels on the efficiency of biophotovoltaic (BPV) platforms in generating bioelectricity. When light energy strikes the surface of the photosynthetic apparatus of algal cells, electrons are shuttled from the algal cells to the anode through a mediator but scientific findings have suggested that direct electron transfer from the microalgae to the anode could boost the efficiency of electron transport mechanism in a BPV device by reducing internal resistance (Ng *et al.*, 2014a). In this study, mediator-less anodes were adopted in the BPV devices by growing algal biofilms from suspension and immobilized *Chlorella* sp. (UMACC 313) cultures on ITO-coated glass anodes. Immobilized cultures were prepared by entrapping the microalgal cells in 2% sodium alginate solution. The BPV devices were illuminated by four different irradiance levels (30, 90, 150 and 210 μmol photons $m^{-2}\,s^{-1}$) to investigate the relationship between varying irradiance levels on the power output of the devices. Photosynthetic performance of the microalgal cells was evaluated using Pulse Amplitude Modulation Fluorometer (PAM) on Days 0, 4, 8 and 12 of the experiment whereas power output of the BPV devices were found from polarization curves generated by applying external resistance stepping technique (Ng *et al.*, 2017). The maximum power density and maximum current density were produced from alginate-immobilized biofilms at the irradiance level of 150 μmol photons $m^{-2}\,s^{-1}$. High Non-Photochemical Quenching (NPQ) readings at 150 μmol photons $m^{-2}\,s^{-1}$ indicated effective photoprotection in Photosystem II (PS II) that prevents inactivitation of PS II when exposed to strong irradiance. The lowest power output from

immobilized cultures was recorded at 210 µmol photons m^{-2} s^{-1}, thus suggesting that partial photoinhibition had occurred at high irradiance level.

Keywords: irradiance, bioelectricity, BPV device, microalgae

KESAN TAHAP IRADIASI YANG BERBEZA PADA PENJANAAN

BIOELEKTRIK DARIPADA PERANTI-PERANTI *BIOPHOTOVOLTAIC*

ALGA

ABSTRAK

Organisma yang menjalankan proses fotosintesis termasuk mikroalga terdedah kepada tahap iradiasi cahaya matahari yang berubah-ubah sepanjang hari. Fakta ini mencetuskan minat saintis untuk membuat penyelidikan dalam kesan tahap iradiasi cahaya yang berbeza terhadap kecekapan alat *biophotovoltaic* (BPV) dalam penjanaan kuasa bioelektrik. Apabila tenaga cahaya menyinari permukaan radas fotosintesis dalam sel-sel alga, elektron-elektron akan dipindahkan dari sel-sel mikroalga ke permukaan anod melalui sebatian pengantara tetapi kajian saintifik menunjukkan bahawa pemindahan elektron secara langsung dari mikroalga ke anod boleh meningkatkan keberkesanan mekanisma pemindahan elektron dalam alat-alat BPV dengan mengurangkan rintangan dalaman. Dalam projek ini, anod tanpa sebatian pengantara telah diaplikasikan dalam alat BPV dengan pembentukan biofilem alga daripada kultur alga *Chlorella* sp. (UMACC 313) ampaian dan kultur alga *Chlorella* sp. terperangkap dalam alginat pada permukaan anod kaca bersalut Indium Tin Oxide (ITO). Alga diperangkap dalam alginat dengan menggunakan 2% larutan natrium alginat. Mikroalga dalam alat BPV kemudian diterangi oleh empat tahap iradiasi cahaya iaitu 30, 90, 150 dan 210 μmol photons m^{-2} s^{-1} untuk menyiasat hubungan antara tahap iradiasi yang berlainan dengan penjanaan kuasa oleh alat BPV tersebut. Prestasi fotosintesis sel-sel mikroalga dinilai menggunakan *Pulse Amplitude Modulation Fluorometer* (PAM) pada 0, 4, 8 dan 12 hari eksperimen manakala penjanaan kuasa oleh alat-alat BPV ditentukan daripada lengkung polarisasi yang dihasilkan menggunakan teknik langkauan rintangan luaran. Densiti kuasa maksimum and densiti arus maksimum dijana oleh biofilem dalam bentuk kultur alga yang terperangkap dalam alginat pada tahap iradiasi 150 μmol photons m^{-2} s^{-1}. Nilai-nilai *Non-*

Photochemical Quenching (NPQ) pada tahap sinaran yang sama menunjukkan mekanisma pelindungan fotosistem II yang efektif daripada cahaya yang berlebihan telah mengelakkan berlakunya penyahaktifan fotosistem II apabila terdedah pada tahap iradiasi yang kuat. Ketumpatan kuasa maksimum yang paling rendah pada 210 μmol photons m^{-2} s^{-1} menunjukkan bahawa proses penyekatan cahaya dalam sel-sel mikroalga telah berlaku.

Kata kunci: sinaran, bioelektrik, peranti BPV, mikroalga

ACKNOWLEDGEMENTS

First and foremost, I would like to express my utmost gratitude to my supervisor, Prof. Dr. Phang Siew Moi for giving me an opportunity to join her lab and for giving me continuous support, advices and encouragement throughout my research project. Despite the pressure of keeping up to her expectations, she would constantly offer me useful advice so that I will never stop trying to improve myself as a student and a researcher. I am also thankful to have Prof. Dr. Ling Tau Chuan as my co-supervisor as he is always amicable and ready to assist me whenever I needed help in my project.

Next, I would like to thank Dr. Ng Fong Lee for her guidance, assistance, support and faith in me from the beginning of my project itself. She would always try her best to assist me and was never selfish in sharing her knowledge and expertise. Without having her as my mentor, I would not have been able to complete this project.

Besides, I am grateful for the presence of my seniors and fellow lab members, Dr. Yeong Hui Yin, Dr. Vejeysri Vello, Lee Kok Keong, Lim Shin Jing, Tan Yong Hao and the rest. Their warm and kind personalities helped me to tackle challenges in my project and made my time spent in the lab memorable.

Last but not least, I can never thank my parents and sister enough for their unconditional love and sacrifices in ensuring that I am able to complete this project. They were and will always be my motivation to work hard and make them proud with my achievement.

TABLE OF CONTENTS

LIST OF FIGURES

LIST OF TABLES

LIST OF SYMBOLS AND ABBREVIATIONS

α	:	Light harvesting efficiency
μ	:	Specific growth rate
°C	:	Degree Celcius
d^{-1}	:	Per day
ΔpH	:	pH gradient
M	:	Molar
mAm^{-2}	:	Milliampere per square meter
mg chl-*a* L^{-1}	:	Milligram chlorophyll-a per liter
mV	:	Millivolt
mWm^{-2}	:	Milliwatt per square meter
mWm^{-2} mg chl-a^{-1}	:	Milliwatt per square meter per milligram chlorophyll-*a*
μmol electrons $m^{-2}s^{-1}$	:	Micromol electrons per square meter per second
μmol photons $m^{-2}s^{-1}$	:	Micromol photons per square meter per second
rpm	:	Rotations per minute
V	:	Volt
ATP	:	Adenosine triphosphate
BBM	:	Bold's Basal Medium
BPV	:	Biophotovoltaic
$CaCl_2$	:	Calcium chloride
Chl-*a*	:	Chlorophyll-*a*
CO_2	:	Carbon dioxide
$Cytb_6f$	:	Cytochrome b_6f complex
DET	:	Direct electron transfer
E_k	:	Photoadaptive index
F_m	:	Maximum fluorescence value

F_o	:	Minimum fluorescence value
F_v	:	Variable fluorescence value
F_v/F_m	:	Maximum quantum efficiency
H_2O_2	:	Hydrogen peroxide
ITO	:	Indium tin oxide
LED	:	Light-emitting diode
LHCs	:	Light harvesting complexes
MFC	:	Microbial fuel cell
$NADP^+$	:	Nicotinamide adenine dinucleotide phosphate
NADPH	:	Dihydronicotinamide adenine dinucleotide phosphate
NPQ	:	Non-photochemical quenching
OCP	:	Open circuit potential
OD_{620nm}	:	Optical density at 620 nanometers
OD_{630nm}	:	Optical density at 630 nanometers
OD_{645nm}	:	Optical density at 645 nanometers
OD_{665nm}	:	Optical density at 665 nanometers
OEC	:	Oxygen-evolving complex
P_{680}	:	Photosystem II primary electron donor
PAM	:	Pulse amplitude modulation
PDMS	:	Polydimethylsiloxane
PQH_2	:	Plastoquinol
PSI	:	Photosystem I
PSII	:	Photosystem II
Q_A	:	First quinone acceptor
Q_B	:	Secondary plastoquinone molecule
qE	:	Energy-dependent quenching

qI	:	Photoinhibitory quenching
Q_o	:	Quinol-oxidation
qT	:	State-transitioning quenching
qZ	:	Zeaxanthin-based quenching
rETR	:	Relative electron transport rate
$rETR_{max}$	:	Maximum relative electron transport rate
RLC	:	Rapid light curve
ROS	:	Reactive oxygen species
SGR	:	Specific growth rate
UMACC	:	University of Malaya Culture Collection

LIST OF APPENDICES

CHAPTER 1: INTRODUCTION

1.1 Background

Efforts to develop sustainable energy have intensified in recent years to fulfill the needs of rapid population and economic growth, while simultaneously minimize the risk of exhausting natural fuel resources to the core. Although awareness on the importance of reverting to cleaner forms of energy is no longer lacking, massive deforestations and fossil fuel combustions in the past had pushed global carbon concentrations beyond the sustainable level. To date, it is still improbable for renewable energy to completely eliminate our dependence on fossil fuels. In certain places, installation of state-of-the-art infrastructure for renewable energy generation remains a challenge in terms of spatial, economic and technical feasibility. The energy that the earth receives from the sun in an hour exceeds mankind's annual total energy consumption (Lewis & Nocera, 2006). Therefore, only a small percentage of sunlight is required to sustain the energy needs worldwide (Nishio *et al.*, 2010). As a result, wide attention is drawn to sunlight as a reliable source for bioenergy production.

Biophotovoltaic (BPV) cells were one of the novel ideas to convert sunlight into useful energy. One of the key components of a BPV device is the photoautotrophic microorganisms that convert solar energy to electricity with zero carbon footprint (Zou *et al.*, 2009). BPV platforms that contain live photosynthetic organisms such as algae and cyanobacteria have been shown to generate bioelectricity through the process of photosynthesis (Bombelli *et al.*, 2014; McCormick *et al.*, 2011; Ng *et al.*, 2014a; Ng *et al.*, 2014b, 2017). BPV devices are regularly compared and contrasted with microbial fuel cells (MFCs) due to the many similarities and differences between the two types of fuel cells. MFCs are able to generate significantly higher bioelectricity than BPV devices although magnitude of power output is largely dependent on the type of electrodes used.

However, the advantages of BPV cells over MFCs in certain aspects make BPV devices equally competitive in fuel cell technology. First, the BPV and MFC hybrid commonly known as Microalgae-MFC eliminates the need to provide aeration in the fuel cell (Fischer, 2018). In fact, the ability of algal BPV devices to capture carbon for algal photosynthesis distinguishes BPV devices from MFCs containing heterotrophic bacteria that are incapable of fixing carbon (Schneider *et al.*, 2016).

Most algal BPV devices contain suspension algal cultures that form algal biofilms on the surface of the anode. Biofilm formation is dependent on both the characteristics of the cells and the electrode surface which include surface roughness and surface energy (Bombelli *et al.*, 2012). Guo (2014) found that electrodes with hydrophilic surfaces are favored for biofilm development in electrochemical systems but Choudhury *et al.* (2016) found that biofilm growth was more apparent on a surface with strong hydrophobicity while hydrophilic surface was more fitting for enhancing electrochemical activities. Since the number of variables that can affect the process of biofilm formation is big, the introduction of cell immobilization into algal BPV devices will help tackle some of the challenges associated with suspension cultures. Algal cell immobilization is commonly done using natural gel-like substances such as chitosan, carrageenan, alginate and agarose (Guisan, 2006). In spite of the shortcomings of cell immobilization in algal BPV devices that should be addressed, the entrapment of algal cells within the gel matrix concentrates cell colonies on the top surface for maximum light absorption. Algal immobilization further improves the contact between algal cells and the electrode surfaces for efficient electron transfer between the two interfaces when the algal cells are 'locked' right on top of the electrode surfaces.

The process of bioelectricity generation from algal BPV devices initiates from the moment light hits the surface of the algal cells. Microalgae may have refined capacity to adjust to the amount of light received but the lethal effects of exposure to high irradiance for extended periods of time sometimes dominate over the algal photoprotective mechanism. Although most photoautotrophic organisms including microalgae are able to recover from minor photo-induced damages, the cessation in photosynthetic energy conversion during photoinhibition period will debilitate power output from algal BPV devices. Therefore, the aim of this research work is to investigate and identify the optimum irradiance level for suspension and immobilized *Chlorella* sp. cultures in flat-plate algal BPV devices so that maximum power output can be attained within the photosynthetic capacity of the microalgae. The research outputs will make significant contributions to future work on optimizing power output from algal BPV devices.

1.2 Research Questions

(1) Would the use of immobilized cultures in algal BPV devices increase power output compared with suspension cultures?

(2) Does power output from algal BPV devices increase with increasing irradiance that the algal cells are exposed to?

1.3 Research Objectives

(1) To investigate the feasibility of utilizing an alginate-immobilized algal biofilm in enhancing photosynthetic performance and power output in algal BPV devices.

(2) To study the effect of different irradiance levels on the photosynthetic performance and power output in algal BPV devices.

CHAPTER 2: LITERATURE REVIEW

2.1 Photosynthesis

Photosynthesis is a natural process that converts light energy into chemical energy by photosynthetic organisms to produce sugar from carbon dioxide and water (Bard & Fox, 1995). Light exists in the form of electromagnetic radiation with a visible light spectrum that ranges in wavelengths between 400 nm and 700 nm (Masojídek *et al.*, 2013). However, not all photons within the visible light spectrum are utilized to break the covalent bond between oxygen and hydrogen atoms in water molecules. The approximate amount of energy required for water splitting is 1.8 eV which is parallel with the energy level in the red region of the spectrum (Barber, 2009).
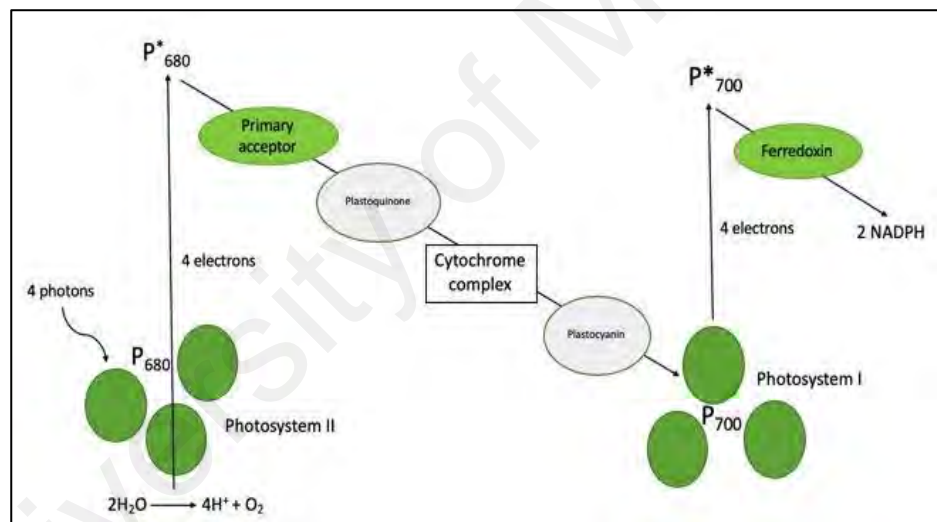
Figure 2.1: Electron Pathway in the Photosynthetic Electron Transport Chain.

During photosynthesis, the energy from light photons splits water into molecular oxygen, protons and electrons in the PSII oxygen-evolving complex (OEC) which is made up of tetramanganese atoms, calcium ion, Ca^{2+} and presumably a chloride ion, Cl^- that are chemically bound together to the core protein complexes (McEvoy *et al.*, 2005). Light energy is absorbed by chlorophyll binding proteins and channeled to the Photosystem II (PSII) primary electron donor, P_{680} (Masojídek *et al.*, 2013; Rögner *et al.*, 1996). The charge separation phenomenon between Chl_{D1} and pheophytin, $Pheo_{D1}$

precedes reduction of the primary electron acceptor, Q_A which in turn transfers two electrons to the secondary plastoquinone molecule, Q_B (Liu *et al.*, 2018; Masojídek *et al.*, 2013). Q_B is dislodged from PSII after turning into a plastoquinol (PQH_2) upon double reduction to arrive at the quinol-oxidation (Q_o) site of the cytochrome b_6f complex ($Cytb_6f$) for oxidation to ensue (Rochaix, 2011). At the same time, the protons discharged from the water splitting reaction are counterbalanced by the proton uptake on the stromal side for re-oxidation of PQH_2 (Murray & Barber, 2007). From the Cyt b_6f complex, plastocyanin acts as a mediator for electron transfer to Photosystem I (PSI) where electrons are then subsequently transferred to ferredoxin for $NADP^+$ reduction to NADPH (Van Eerden *et al.*, 2017). The combination of proton and electron exchanges across the thylakoid lumen develops an electrochemical potential gradient of protons for ATP synthesis (Murray & Barber, 2007; Rochaix, 2011). NADPH coupled with ATP are involved in the carbohydrate manufacturing from carbon dioxide, CO_2 in the Calvin Benson cycle (Johnson, 2016).

Photosynthesis is limited by various factors, mainly temperature, light, pH, salinity, carbon dioxide and nutrients (Gatamaneni *et al.*, 2018). The change in temperature influences microalgal growth, as the most suitable temperature range for microalgal cultivation was reported to fall between 15ºC and 30ºC (Singh & Singh, 2015). Increase in temperature promotes microalgal growth through increased enzymatic activities in the Calvin cycle. However, temperatures above 40ºC impede PSII activity and cell division in most microalgal species when charge separation in PSII is hindered and reactive oxygen species (ROS) is produced from the failure of PSII to evolve oxygen (Ras *et al.*, 2013). Salt concentration, on the other hand, regulate physiological and biochemical processes for cell growth in microalgae (Mohan & Devi, 2014). Despite the need for chloride ions in adenosine triphosphate and flavin mononucleotide production

through Hill reaction, excessive sodium chloride, NaCl leads to reduced growth rate in algal cultures (Rai *et al.*, 2015).

2.2 Light

In algal culturing, light utilization efficiency is a crucial parameter in regulating the photosynthetic efficiency of the algal cells (Neidhardt *et al.*, 1998). Hu and Richmond (1996) suggested that light intensity is proportional to algal concentration and biomass production. Despite the importance of irradiance on photosynthetic performance of microalgae, identification of the optimum irradiance level for each species is crucial to prevent excessive light energy from instigating oxidative damage on PSII and subsequently, cellular death (Carvalho *et al.*, 2011).

Excess light energy in photosynthetic organisms is dissipated via three pathways: reemission as fluorescence, thermal dispersion and conversion of chlorophyll-*a* (chl-*a*) molecule to its triplet state (Maxwell & Johnson, 2000). The triplet state carries the risk of inducing the formation of harmful ROS when energy is passed to ground-state oxygen from the chl-*a* molecule (Muller *et al.*, 2001). An oxygen molecule needs to accept four electrons to produce two water molecules during aerobic metabolism but quad-electron acceptance takes place stepwise as spin restrictions accommodate only a single electron at a time (Mallick & Mohn, 2000). When a stable ground state oxygen undergoes reduction, the energy input to oxygen develops the intermediate singlet oxygen whereas electron transfer leads to undesirable formation of superoxide anion, hydrogen peroxide and hydroxyl radicals (Apel & Hirt, 2004; Latifi *et al.*, 2009). The thylakoid membranes are the defending grounds against photooxidative damages induced by singlet oxygen with carotenoids providing the first protective layer through effective singlet oxygen quenching near the light harvesting complexes (LHCs) and photosynthetic reaction centers in the photosystems (Ksas *et al.*, 2015). Similarly, topopherols are light-dependent

proteins that also serve as singlet oxygen quenchers to protect D1 protein from high irradiance damages and prevent photoinhibition in algae (Trebst *et al.*, 2002).

Non-Photochemical Quenching (NPQ) involves dissipation of surplus light energy in the form of heat to prevent the PSII photosynthetic apparatuses from overexcitation (Lambrev *et al.*, 2012). NPQ comprises of various separate regulatory mechanisms i.e. energy-dependent dissipation in the PSII antenna known as qE (Krause *et al.*, 1982), state transition quenching, qT, photoinhibitory quenching, qI (Muller *et al.*, 2001) and zeaxanthin-based quenching, qZ (Nilkens *et al.*, 2010). The key component of NPQ, qE is piloted by regulation of the xanthophyll cycle in which zeaxanthin is made from violaxanthin through anteraxanthin (Demmig-Adams & Adams, 1996). Once the saturating limit of ΔpH is reached, approximately 80% of variable fluorescence is estimated to be expelled (Krause, 1988). Although the forward reaction of qE is driven by the trans-thylakoid pH gradient, reliance of PSII antenna quenching on ΔpH expires when zeaxanthin is reserved in the system (Quaas *et al.*, 2015). When thermal dissipation occurs, observations of a decline in photochemical efficiency of PS II is projected (Demmig-Adams & Adams, 2003). The surge in zeaxanthin level precedes a lower quantum yield output (Kato *et al.*, 2003), as photochemical quenching, by theory, is null when PSII reaction centers are closed or when the plastoquinone Q_A is in its reduced form (Lambrev *et al.*, 2012).

At high irradiance levels, photoinhibition may also take place as algal cells in the upper layers receive excessive illumination whereas the cells in the lower layers are light-deprived when light is attenuated as it penetrates deeper into the cells (Mitra & Melis, 2008), resulting in reduced biomass production (Amini Khoeyi *et al.*, 2012). Continuous exposure to high irradiance further damages PSII apparatuses which leads to buildup of these impaired units and failure in piloting charge separation within the photosystem

(Smith *et al.*, 1990). Certain literature termed photoinhibition as imbalance between the rate of repair of damaged PSII and the rate at which the D1 protein in the PSII reaction center is degraded by excess light (Murata *et al.*, 2012; Nishiyama *et al.*, 2004; Takahashi & Badger, 2011). Identification of photo-induced damages on PSII is affirmed when protein synthesis inhibitors such as lincomycin and chloramphenicol are detected whereas the extent of PSII recovery from the damages is gauged by PSII activity after transferal from high to low light intensity (Murata *et al.*, 2012). Although photoinhibition takes place in a broad array of light levels (Roach & Krieger-Liszkay, 2014), high light intensities are accountable for inhibition of electron flow from pheophythin to the twice reduced first quinone acceptor, Q_A (Styring *et al.*, 1990). The capturing of excessive light brings forth the combined effects of doubly reduced Q_A and formation of P_{680} in its triplet state which hinders the forward electron transfer process from PSII to PSI (Krieger-Liszkay *et al.*, 2008). Nevertheless, light is not essential during the degradation process as it acts only as an activator for D1 proteolysis (Andersson *et al.*, 1992). Photoinhibition is hastened when D1 protein synthesis is disrupted by $NADP^+$ drainage, followed by formation of excessive H_2O_2 that suppresses PSII reparation (Takahashi & Murata, 2008). Once D1 protein phosphorylation fails to proceed for *de novo* synthesis of D1 protein for PSII repair (Aro *et al.*, 1993), the prolonged rate of PSII repair significantly affects photosynthetic activity in the algal cells, resulting in weak electron transport in PSII and poor power output from the BPV devices. When photosynthetic performance is hampered by irradiance, bioelectricity generation from BPV devices will be significantly impacted, thus thorough understanding of the irradiance effect on algal photosynthesis in BPV devices is essential.

2.3 Algal Biophotovoltaic Device

A biophotovoltaic cell (BPV) consists of photoautotrophic organisms such as algae and cyanobacteria that capture light energy to convert carbon dioxide and water into organic matter and oxygen. A BPV device works in a similar manner as a conventional microbial fuel cell (MFC) except that electrons deposited on the anode of a BPV device come from a photosynthesis process instead of from the breakdown of organic matter by bacteria. During photosynthesis, organic compounds are made (Xu, 2015) while in the chloroplasts, water molecules are split into protons, electrons and oxygen through photolysis (Pinhassi *et al.*, 2016). The light energy absorbed excites chlorophyll molecules to its excited singlet state; electrons from this singlet state flow to the reaction centers for charge separation to take place (Brotosudarmo *et al.*, 2014; Masojídek *et al.*, 2013). However, in a BPV device, some electrons are attracted to the anode and flow to the cathode along an external circuit, thus generating bioelectricity (Mao & Verwoerd, 2013; Saar *et al.*, 2018).

Electrons can be ferried from biological cells to the anode via three different major pathways: (i) direct electron transfer (DET) from exo-electrogens such as c-type cytochromes to the anode surface; (ii) through an endogenous electron transfer mediator such as Flavin or (iii) through an exogenous electron transfer mediator such as polypyrrole and polyaniline (Bosire & Rosenbaum, 2017; Ng *et al.*, 2017; Yong *et al.*, 2014). Qiao *et al.* (2010) implied that MFCs without exogenous mediators were gaining popularity due to apparent downsides of mediators. The use of artificial redox mediators in fuel cell technology was deemed impractical due to the unsustainable quality of the mediators (Rosenbaum *et al.*, 2010). Hence, fuel cell technology slowly shifts from mediator-based anodes to mediator-less anodes when improvements in terms of device efficiency and simplicity were exhibited with the absence of redox mediators (Bombelli

et al., 2014). DET eliminates the setback in electron transfer efficiency that results from discharging by separate mediators at the same electrode or ion neutralization through charge transfer to a neutral atom in the electrolyte (Mahmoudzadeh et al., 2011). Carmona-Martínez et al. (2013) described the ferrying of electrons through redox protein in the cell membrane or extracellular bacterial appendages known as nanowires as part of the electron transport mechanism from living cells to MFC electrodes. In spite of the various electron transfer mechanisms proposed, explanation on why electrons from photolysis of water are attracted to the anode is still lacking in lucidity. A possible explanation is reflected in the work of Pisciotta et al. (2011) who suggested that electron transfer from biological cells to the external environment impedes plastoquinone pools from accepting too much electrons under excessive illumination conditions. Although DET seems more advantageous than mediator-assisted transfer, Saper et al. (2018) reasoned that the amount of electric current generated is circumscribed by the monolayer algal cells in contact with the electrode. In addition, the right cell orientation is also an essentiality in boosting interaction between the active site of the cells and the electrode surface (Freire et al., 2003). Since DET involves no exogenous mediator to facilitate electron transfer, efficient electron transfer from the cells to the electrode is a function of surface roughness of the accepting electrode which determines the extent of cell attachment on the electrode (Schneider et al., 2016).

2.4 Alginate and Algal Immobilization

Early algal BPV devices used suspension algal cultures for formation of algal biofilms (McCormick et al., 2011; Ng et al., 2014b) but algal immobilization in alginate had shown enhancement in power output from BPV devices. Alginate is a biopolymeric chain that contains α-L-guluronic acid and (1,4)-linked ß-D-mannuronic acid (Bayramoğlu et al., 2006; Devrimci et al., 2012; Ertesvåg & Valla, 1998; Kim et al.,

2011; Pathak *et al.*, 2008; Pawar & Edgar, 2012; Schmid *et al.*, 2008). Algal immobilization is practiced for biomass retention, tolerance against chemical toxicity and user-friendliness (de-Bashan & Bashan, 2010). The α-L-guluronic acid residues known as G-block formulate gel beads by bonding with divalent ions (Moreira *et al.*, 2006), thus making alginate a highly feasible immobilization material for microalgae (Martinsen *et al.*, 1989).

An observable advantage of immobilizing microalgae within the alginate gel matrix is that it provides a protective shield over encapsulated microalgae cells against external stress factors that could inhibit cellular growth and activities (Yabur *et al.*, 2007; Zhu & Yang, 2007). In other words, cell immobilization helps to keep algal health in check by forming a barrier between the algal cells and toxic substances that could be ruinous to the cells. As the basis for increased biomass productivity and photosynthetic performance lies within the positive physiological state of the algal cells, cell immobilization will then be uplifting operational stability of the algal cells (Das & Adholeya, 2015). Apart from deterring negative implications of fluctuating physico-chemical conditions on microalgae through immobilization, the idea of immobilizing microalgae with alginate introduces the possibility of higher desirable photosynthetic outcome. Immobilized algal cells are disengaged from prolonged non-productive growth phase; thus, the extended cell activity and productivity of the immobilized algal cells lead to upsurge in production yield (Zhu & Yang, 2007).

CHAPTER 3: METHODOLOGY

3.1 Algal Culture

The algal strain selected for this project was the *Chlorella* UMACC 313 from the University of Malaya Culture Collection (UMACC). *Chlorella* UMACC 313 was isolated from a treatment pond of palm oil mill effluent. The methods of preparing and maintaining the algal cultures were adapted from ("Biohybrid Photoprotein-Semiconductor Cells with Deep-Lying Redox Shuttles Achieve a 0.7 V Photovoltage," 2017; Ng *et al.*, 2014a; Ng *et al.*, 2017). The inoculum size used was 20%, prepared from exponential phase algal cultures that were standardized at $OD_{620nm}=2.0$. The algal cultures, grown in Bold's Basal Medium (Nichols & Bold, 1965) in 500 mL conical flasks, were placed on an incubator shaker (130 rpm) at a temperature of $25\pm1\ °C$ and an irradiance level of 30 µmol photons $m^{-2}\ s^{-1}$ on a 12:12 light-dark cycle.

3.2 Immobilization of Algal Cells

Immobilization of the *Chlorella* cells was done with sodium alginate powder (purchased from Natural Colloids Industries Pte. Ltd.). The algal cells were immobilized in 2% sodium alginate. 4 g of 2% sodium alginate powder were weighed out and added into 190 mL of sterile distilled water to prepare sodium alginate solution (Ng *et al.*, 2017). After placing a 50 mm sterile magnetic stirrer bar into the mixture, it was placed on a magnetic stirrer for continuous stirring over a duration of 24 hours.

The algal culture containing cells from the logarithmic growth phase was centrifuged in 15 mL conical centrifuge tubes (Falcon) at 3000 rpm for 10 minutes. The supernatants were removed and the concentrated algal cells were resuspended in BBM to prepare an algal suspension of $OD_{620} = 2.0$. 10 mL of the algal suspension were added to the 190 mL sodium alginate solution to form an algal alginate suspension.

Three mL of the algal alginate suspension was pipetted and spread onto ITO-coated glass slides (KINTEC, Hong Kong) of dimension 3.5 cm x 3.5 cm and layer thickness of 100 nm (Ng *et al.*, 2017). The ITO-coated glass with the algal-alginate layer was set aside for a minimum of 15 minutes to allow the algal alginate suspension to settle on the glass surface (Ng *et al.*, 2017). The gelation process of the algal alginate suspension was completed by spraying 0.5 mL sterile calcium chloride, $CaCl_2$ (0.1 M) solution on its entire surface (Ng *et al.*, 2017). Sterile distilled water was used to rinse the surface of the gel film to remove the $CaCl_2$ solution after the culture immobilization process was completed.

3.3 Irradiance Experiments: Algal BPV Devices and Experimental Design
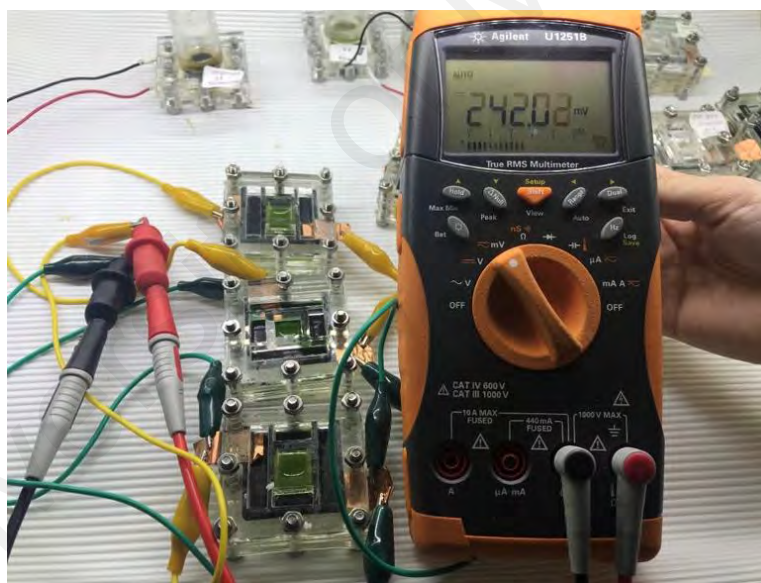
Figure 3.1: Flat-Plate Algal BPV Devices in Triplicates for Power Measurement.

Each of the algal BPV devices shown in Figure 3.1 consists of a cathode and an anode made of platinum-coated glass and ITO-coated glass respectively. The ITO anode had immobilized algae attached to its surface and was sealed with polydimethylsiloxane (PDMS) before Bold's Basal Medium was loaded to the set-up (Laohavisit *et al.*, 2015; Ng *et al.*, 2017). The cathode and the anode were separated by a Perspex piece (Laohavisit

et al., 2015; Ng *et al.*, 2014a; Ng *et al.*, 2014b). Crocodile clips and copper wires were used to connect the anode and cathode to the external circuit.
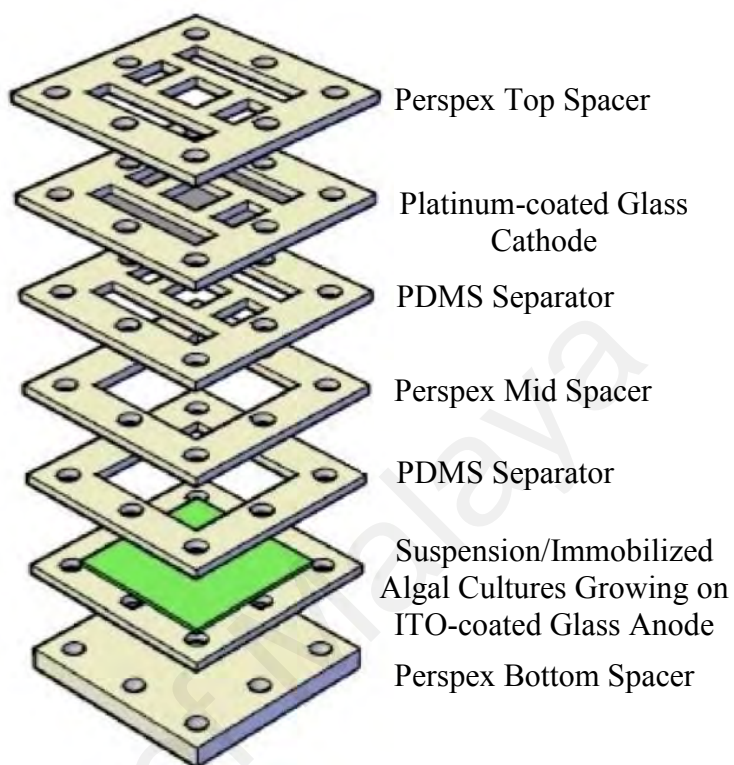
Figure 3.2: Design of Algal BPV Devices Used in the Present Study (Reproduced with permission from Ng *et al.*, 2017).

To investigate the effect of irradiance on growth of the algae and power output, the algal BPV devices were placed in an incubator under white LED lights with irradiance levels of 30, 90, 150 and 210 μmol photons m^{-2} s^{-1} throughout three different sets of experiments. Set 1 consisted of the control irradiance of 30 μmol photons m^{-2} s^{-1} compared with 90 μmol photons m^{-2} s^{-1}. Set 2 consisted of the control irradiance of 30 μmol photons m^{-2} s^{-1} compared with 150 μmol photons m^{-2} s^{-1}. Set 3 consisted of the control irradiance of 30 μmol photons m^{-2} s^{-1} compared with 210 μmol photons m^{-2} s^{-1}. The temperature in the incubator was monitored with a temperature and light data logger (HOBO Pendant®) and was maintained at 25±1°C. Irradiance was measured at the

surface of the algal-alginate films using a light meter (LI-COR LI-250A). The experimental design in this study is shown in the following flow-chart (Figure 3.3).

Preparation of algal culture (UMACC 313)

⬇

Algal immobilization using alginate on ITO-coated glass

⬇

Algal BPV devices setup

⬇

Experiment: Effect of Different Irradiance levels on Bioelectricity Generation from Algal BPV Devices

⬇   ⬇

Photosynthetic performance (PAM Fluorometry and Spectrophotometry)   Power output

⬇

3 Sets of Experiments: Set 1 (30 and 90 μmol photons m^{-2} s^{-1})
Set 2 (30 and 150 μmol photons m^{-2} s^{-1})
Set 3 (30 and 210 μmol photons m^{-2} s^{-1})

⬇

Data collection and analysis

⬇

Thesis writing and submission

Figure 3.3: Flow Chart Showing the Experimental Design in this Study.

3.4 Determination of Chlorophyll *a* and Carotenoid Contents, Biomass and Specific Growth Rate

The chl-*a* content of the algal cells was used to estimate biomass. Chl-*a* was determined on days 0, 4, 8 and 12. The suspension culture was filtered through glass-fiber filter papers (Whatman GF/C, 0.45 μm) to separate the algae from the medium. The filter papers with suspended algal cells on the surface were grinded into small pieces with a tissue grinder (Kimble, USA) before being transferred into a 15 mL Falcon centrifuge tubes. 10 mL of analytical grade 100% acetone were pipetted into the centrifuge tubes. The centrifuge tubes were immediately wrapped with aluminum foil and stored in the freezer at a temperature of 4 °C for 24 hours. The samples were centrifuged at 3000 rpm for 10 minutes. 1 mL of sample from each centrifuge tube was drawn into a cuvette in order to determine the chl-*a* content of the cells through spectrophotometry (Strickland & Parsons, 1972). The samples were analyzed at three different wavelengths: 630 nm (OD_{630}), 645 nm (OD_{645}) and 665 nm (OD_{665}). The chl-*a* content of immobilized algal cells was determined by first releasing the cells from algal gel film through mashing in a tissue grinder after the film was gently removed from the surface of the ITO-coated anode with forceps. The samples were transferred to centrifuge tubes and 10 mL of analytical grade 100% acetone was added into the tubes. The remaining procedures to analyze the chl-*a* content in suspension cultures were carried out for the immobilized algae cells. The formula used to calculate chl-*a* content was as follows (Andersen, 2005):

$$\text{chl} - a \ (\text{mgm}^{-3}) = \frac{(C_A - V_A)}{V_C}$$

where $C_A = 11.6 \times OD_{620nm} - 1.31 \times OD_{645nm} - 0.14 \times OD_{620nm}$

V_A = Volume of acetone (mL) used for chlorophyll extraction

V_C = Volume of algal culture (L)

chl-*a* (mgL^{-1}) = chl-*a* (mgm^{-3})/1000

16

The specific growth rates, SGR (μ) of the algal cultures were determined from the chl-*a* content of the algal cells at exponential growth phase and were calculated with the following formula (Schwartz, 2007):

$$\text{Specific Growth Rate}, \mu \,(d^{-1}) = \frac{(\ln N_2 - \ln N_1)}{t_2 - t_1}$$

where N_2 = chl-*a* content at t_2

N_1 = chl-*a* content at t_1

$t_2 - t_1$ = duration when exponential growth phase occurred

Carotenoids content was estimated using the same extract used for the chl-*a* content estimation as described above. In addition to the wavelengths used for chl-*a* measurement (630 nm, 645 nm and 665 nm), carotenoids content was also determined using the spectrophotometry method with the wavelength of 452 nm. Carotenoids content may be used to indicate stress as it is an anti-oxidant that is involved in photoprotection (Fiedor & Burda, 2018). The formula used to calculate carotenoids content was as follows (Andersen, 2005):

$$\text{Carotenoids} \,(\text{mg L}^{-1}) = \frac{\text{OD}_{452nm} \times 3.86 \times V_e}{V_c}$$

where V_c = Volume of algal culture (L)

V_e = Volume of extract (acetone in mL)

3.5 Electrical Measurements

Power output measurements were taken using a multimeter (Agilent U1251B) with sensitivity of ± 0.001 mV. Resistors of different resistance loads (10MΩ, 5.6MΩ, 2MΩ, 560KΩ, 240KΩ, 62KΩ, 22KΩ, 9.1KΩ, 2.7 KΩ and 910Ω) were applied to the external circuit and by applying Ohm's Law, the polarization curves were generated. The maximum current density and maximum power density were then evaluated from the

polarization curves. A second set of BPV devices using suspension algal cultures with the same cell concentration as the immobilized algae were used for comparison. All experiments were conducted in three individual replicates.

3.6 Pulse Amplitude Modulation (PAM) Fluorometer Measurements

Evaluation on the effects of irradiance levels on the photosynthetic activity of microalgae in BPV devices was conducted using chl-*a* fluorescence data; observations on the changes in chl-*a* fluorescence are performed using the Pulse Amplitude Modulated (PAM) Fluorometry method (Pannier *et al.*, 2014). The photosynthetic parameters that were investigated in this study include maximum quantum efficiency (F_v/F_m), maximum relative electron transport rate ($rETR_{max}$), photoadaptive index (E_k) and Non-Photochemical Quenching (NPQ). All these parameters were measured with a Diving-PAM (Walz, Germany). The algal cultures in the BPV devices were dark-adapted for a minimum of 15 minutes before PAM measurements were made. The minimum fluorescence value (F_o) during the dark adaption process and the maximum fluorescence value (F_m) when the reaction centers are closed after absorption of the energy of a photon were both measured with a PAM Fluorometer (Ciniciato *et al.*, 2016). The variable fluorescence, F_v is the difference between F_m and F_o. The maximum quantum efficiency, F_v/F_m can then be calculated with the following formula:

$$\text{Maximum quantum efficiency}, F_v/F_m = \frac{(F_m - F_o)}{F_m}$$

where F_m = Maximum fluorescence value

F_o = Minimum fluorescence value

Rapid light curves (RLC) were generated when the algae cells were exposed to actinic light emitted by LEDs at different irradiance levels. The initial slope of RLC, α determined the maximum photosynthetic efficiency whereas the product of irradiance and quantum yield measured at the end of the interval determined rETR (Ciniciato *et al.*,

2016; Ng *et al.*, 2014b). E_k was calculated with the formula $rETR_{max}/\alpha$ where $rETR_{max}$ is the maximum photosynthetic rate (Ng *et al.*, 2014b). Excess light energy from photosynthesis will not be stored by photosynthetic plants but it will be converted into heat energy to be released. This phenomenon is expressed in the form of NPQ which can be calculated with the formula $(F_m - F_m')/F_m'$ (Ng *et al.*, 2014b).

3.7 Statistical Approach

All statistical analyses were performed using the Statistica 8 program. Analysis of Variance (ANOVA) followed by Tukey post-hoc test were conducted to determine if there is significant difference within and between the suspension and immobilized cultures at different irradiance levels on Days 0, 4, 8 and 12 of the experiment.

CHAPTER 4: RESULTS

4.1 Growth Curves and Specific Growth Rates

Figure 4.1, Figure 4.2 and Figure 4.3 consist of the growth curves of the suspension and immobilized *Chlorella* sp. cultures at 30 µmol photons $m^{-2} s^{-1}$, 90 µmol photons $m^{-2} s^{-1}$, 150 µmol photons $m^{-2} s^{-1}$ and 210 µmol photons $m^{-2} s^{-1}$. The growth curves display the growth phases of the microalgal cells from the lag phase to the exponential phase and stationary phase respectively.

Figure 4.1: Growth Curve based on chl-*a* content of Suspension and Immobilized *Chlorella* sp. cultures at 30 µmol photons $m^{-2} s^{-1}$ and 90 µmol photons $m^{-2}s^{-1}$. Data as means ± S.D. of three replicates.

Throughout the duration of the experiment, immobilized cultures were able to produce significantly higher (ANOVA, $P<0.05$) biomass (chl-*a*) than suspension cultures at both irradiance levels (30 µmol photons $m^{-2} s^{-1}$ and 90 µmol photons $m^{-2} s^{-1}$) studied in Set 1, signifying better growth performance in the immobilized cultures. In general, the suspension cultures grew slower than the immobilized cultures as the exponential growth

phase of the suspension cultures took place after Day 4 while the exponential growth phase of the immobilized cultures was observed within the first 4 days of the experiment. The chl-*a* content of the immobilized cultures at 30 μmol photons m^{-2} s^{-1} ranged between 0.375±0.056 mg chl-*a* L^{-1} and 12.831±2.562 mg chl-*a* L^{-1} whereas the chl-*a* content of the immobilized cultures at 90 μmol photons m^{-2} s^{-1} ranged between 0.442±0.070 mg chl-*a* L^{-1} and 13.278±2.545 mg chl-*a* L^{-1}. The noticeable difference between immobilized cultures at both irradiance levels is the contrasting growth pattern after Day 8. Instead of dropping after Day 8, the chl-*a* content at 30 μmol photons m^{-2} s^{-1} continued rising until Day 12.

Figure 4.2: Growth Curve based on chl-*a* content of Suspension and Immobilized *Chlorella* sp. cultures at 30 μmol photons m^{-2} s^{-1} and 150 μmol photons m^{-2} s^{-1}. Data as means ± S.D. (n=3).

In the second set of experiment, the suspension cultures at 150 μmol photons m^{-2} s^{-1} had different growth trend from the immobilized cultures. At 150 μmol photons m^{-2} s^{-1}, the suspension cultures exhibited highest growth from Day 0 to Day 4 but the suspension cultures at 30 μmol photons m^{-2} s^{-1} had lower biomass on Day 4 (2.981±0.218

mg chl-*a* L^{-1}) compared to Day 0 (2.985±0.295 mg chl-*a* L^{-1}) before increasing to 3.840±0.671 mg chl-*a* L^{-1} on Day 8 and 5.039±0.874 mg chl-*a* L^{-1} on Day 12. On the other hand, the growth curves of the immobilized cultures at 30 µmol photons m^{-2} s^{-1} and 150 µmol photons m^{-2} s^{-1} showed similar growth patterns with both immobilized cultures showing highest increase of biomass on the first 4 days. The biomass of immobilized cultures at 30 µmol photons m^{-2} s^{-1} increased from 0.429±0.048 mg chl-*a* L^{-1} on Day 0 to 6.629±0.796 mg chl-*a* L^{-1} on Day 4 whereas the biomass of immobilized cultures at 150 µmol photons m^{-2} s^{-1} increased from 0.466±0.020 mg chl-*a* L^{-1} on Day 0 to 6.569±0.589 mg chl-*a* L^{-1} on Day 4.

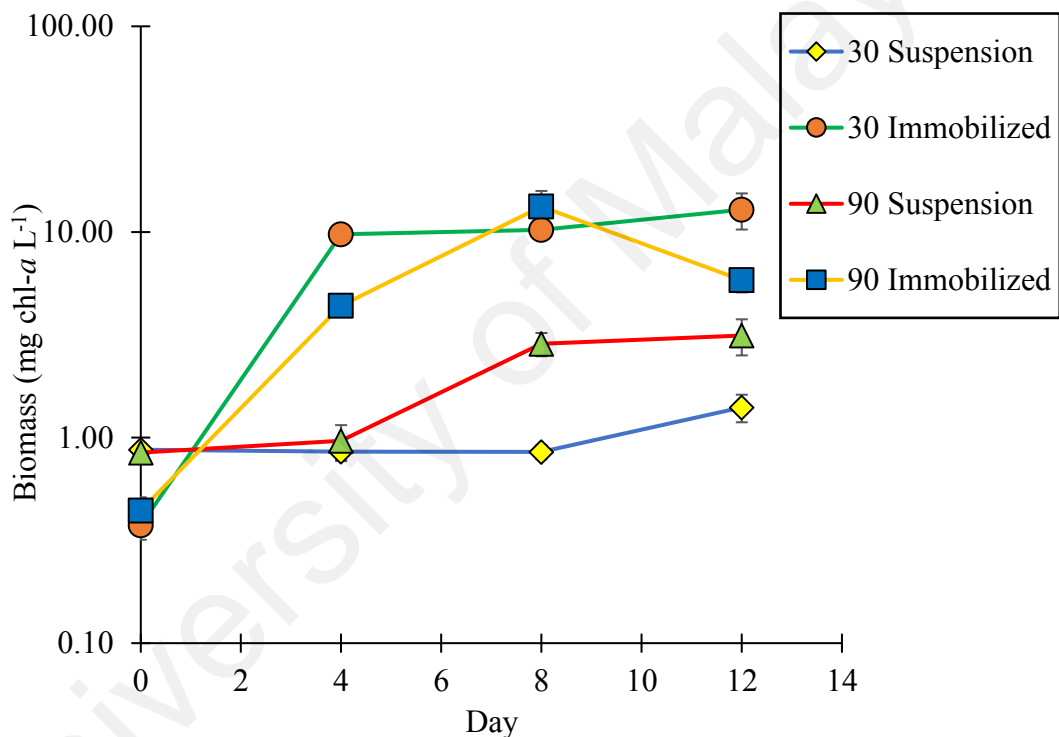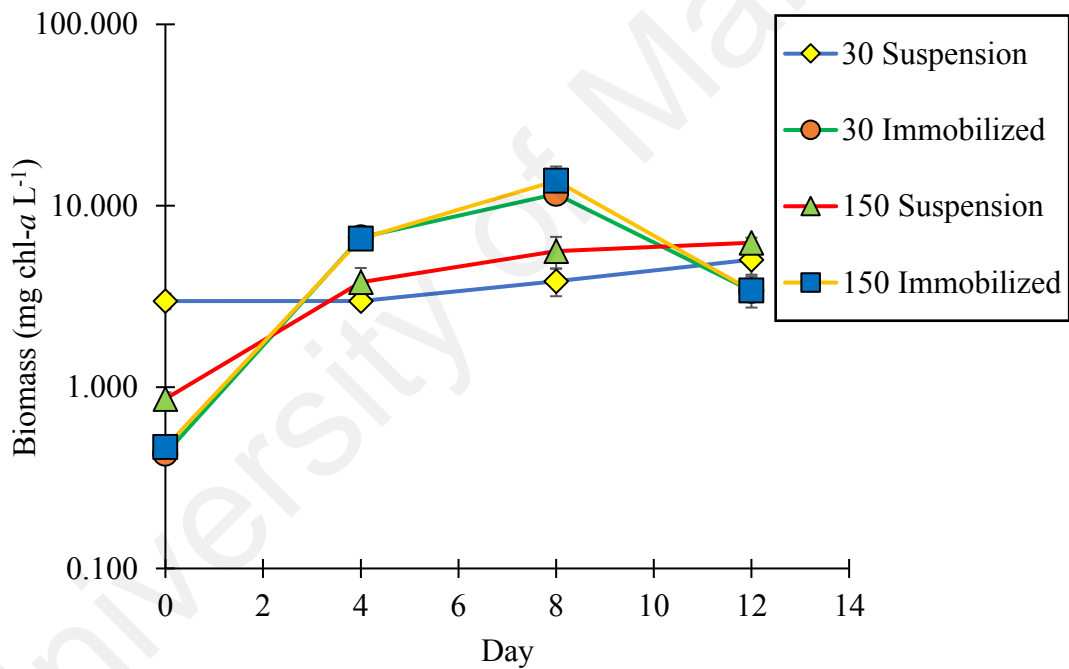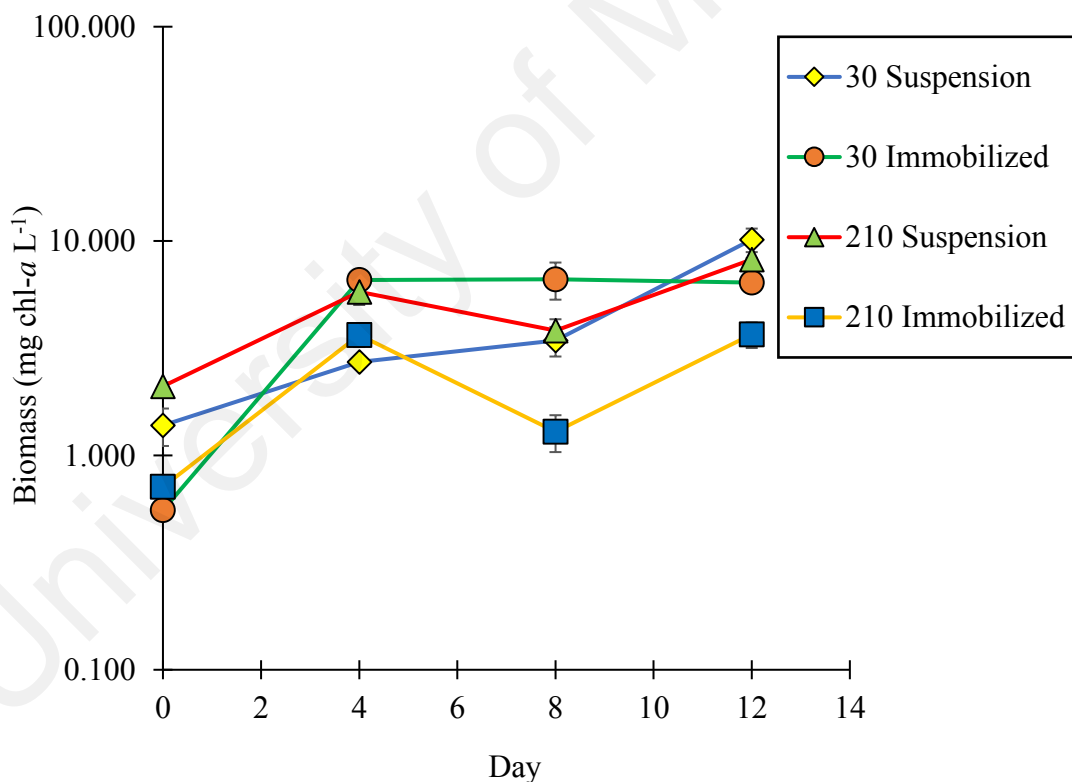**Figure 4.3:** Growth Curve based on chl-*a* content of Suspension and Immobilized *Chlorella* sp. cultures at 30 µmol photons m^{-2} s^{-1} and 210 µmol photons m^{-2} s^{-1}. Data as means ± S.D. (n=3).

The algal cultures at all irradiance levels studied in Set 3 showed positive growth response in the early phase of the experiment. The chl-*a* content of the suspension cultures at 30 μmol photons m^{-2} s^{-1} ranged from 1.381±0.274 mg chl-*a* L^{-1} to 10.157±1.276 mg chl-*a* L^{-1} whereas the suspension cultures at 210 μmol photons m^{-2} s^{-1} had lower biomass ranging between 2.102±0.090 mg chl-*a* L^{-1} and 8.205±0.126 mg chl-*a* L^{-1}. The exponential growth phase of suspension cultures at 30 μmol photons m^{-2} s^{-1} was noticeably delayed, occurring only between Day 8 and Day 12. Immobilized cultures at both 30 μmol photons m^{-2} s^{-1} and 210 μmol photons m^{-2} s^{-1} had lower biomass than the suspension cultures at the same irradiance levels respectively. At 30 μmol photons m^{-2} s^{-1}, chl-*a* content was between 0.555±0.041 mg chl-*a* L^{-1} and 6.634±1.306 mg chl-*a* L^{-1}. The biomass at 210 μmol photons m^{-2} s^{-1} ranged between 0.713±0.093 mg chl-*a* L^{-1} and 3.669±0.499 mg chl-*a* L^{-1}.

In general, the difference in the physiological state of the algal cells led to significant difference (ANOVA, $P<0.05$) in the biomass of suspension and immobilized cultures at 30 μmol photons m^{-2} s^{-1} across Sets 1, 2 and 3 despite exposure to the same irradiance level throughout the study.
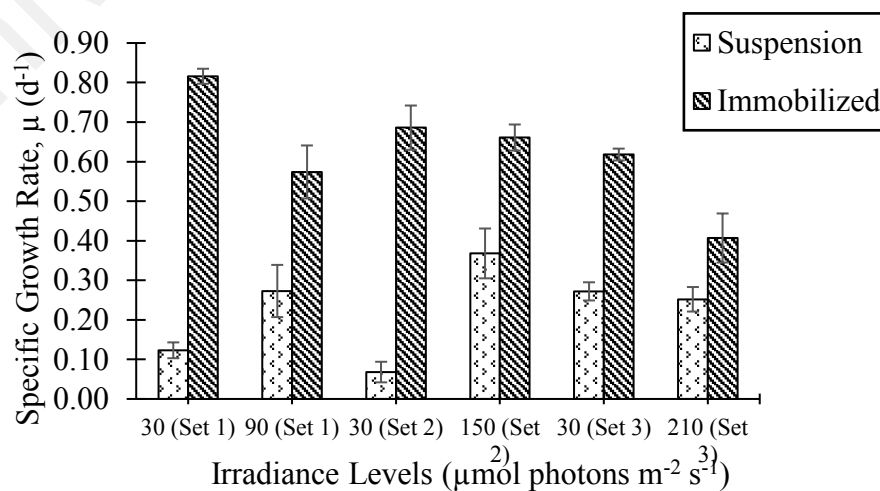
Figure 4.4: Specific Growth Rate, μ of Suspension and Immobilized *Chlorella* sp. cultures at 30, 90, 150 and 210 μmol photons m^{-2} s^{-1}. Data as means ± S.D. (n=3).

In Figure 4.4 above, the SGR of the suspension cultures and immobilized cultures were calculated based on the exponential growth phase of the cultures and were plotted for comparison. In Set 1, the SGR of the suspension cultures increased from 0.123 ± 0.020 d^{-1} to 0.273 ± 0.066 d^{-1} when irradiance increased from 30 μmol photons $m^{-2}\,s^{-1}$ to 90 μmol photons $m^{-2}\,s^{-1}$. Similarly, the SGR in Set 2 was higher at 150 μmol photons $m^{-2}\,s^{-1}$ compared to 30 μmol photons $m^{-2}\,s^{-1}$, increasing from 0.068 ± 0.026 d^{-1} to 0.368 ± 0.063 d^{-1}. However, the drop in specific growth rate from 0.272 ± 0.023 d^{-1} at 30 μmol photons $m^{-2}\,s^{-1}$ to 0.252 ± 0.031 d^{-1} at 210 μmol photons $m^{-2}\,s^{-1}$ signifies lower biomass produced at 210 μmol photons $m^{-2}\,s^{-1}$ per day compared to 30 μmol photons $m^{-2}\,s^{-1}$.

The SGR of the immobilized cultures in Set 1, Set 2 and Set 3 declined when irradiance level increased from 30 μmol photons $m^{-2}\,s^{-1}$ to 90 μmol photons $m^{-2}\,s^{-1}$, 150 μmol photons $m^{-2}\,s^{-1}$ and 210 μmol photons $m^{-2}\,s^{-1}$ respectively. The SGR decreased from 0.816 ± 0.019 d^{-1} to 0.574 ± 0.067 d^{-1} when irradiance was increased from 30 μmol photons $m^{-2}\,s^{-1}$ to 90 μmol photons $m^{-2}\,s^{-1}$. The decrease in SGR was less evident in Set 2 as the SGR dropped slightly from 0.686 ± 0.056 d^{-1} to 0.661 ± 0.033 d^{-1}. As the irradiance was set at 210 μmol photons $m^{-2}\,s^{-1}$, SGR was computed as 0.407 ± 0.062 d^{-1}, significantly lower than the specific growth rate of 0.618 ± 0.015 d^{-1} at 30 μmol photons $m^{-2}s^{-1}$.

4.2 Power Output

At 30 μmol photons $m^{-2}s^{-1}$, the power output of suspension cultures was lower than immobilized cultures on Days 0, 4 and 8 but higher on Day 12. The maximum power outputs generated by suspension cultures and immobilized cultures at 30 μmol photons $m^{-2}s^{-1}$ in the first set of experiment were 0.259 ± 0.016 mWm^{-2} on Day 8 and 0.372 ± 0.031 mWm^{-2} on Day 4 respectively. These values corresponded with current densities of 4.971 ± 0.092 mAm^{-2} and 5.903 ± 0.068 mAm^{-2} respectively. The maximum power outputs of both suspension and immobilized cultures were higher when the BPV devices were irradiated at 90 μmol photons $m^{-2}\,s^{-1}$ compared to 30 μmol photons $m^{-2}\,s^{-1}$. When compared at 90 μmol photons $m^{-2}\,s^{-1}$, immobilized culture was able to yield higher power density than suspension culture. The maximum power density readings of both suspension and immobilized cultures at 90 μmol photons $m^{-2}\,s^{-1}$ were observed on Day 8 at 0.345 ± 0.056 mWm^{-2} and 0.377 ± 0.067 mWm^{-2} respectively. The corresponding current densities for maximum power density readings at 90 μmol photons $m^{-2}\,s^{-1}$ were 5.495 ± 1.057 mAm^{-2} and 5.724 ± 0.399 mAm^{-2} respectively. Between suspension cultures at 30 μmol photons $m^{-2}\,s^{-1}$ and 90 μmol photons $m^{-2}\,s^{-1}$, the maximum power density at 90 μmol photons $m^{-2}\,s^{-1}$ was 33.2% higher than the maximum power density at 30 μmol photons $m^{-2}\,s^{-1}$. The maximum power density margin between immobilized cultures at 30 μmol photons $m^{-2}\,s^{-1}$ and 90 μmol photons $m^{-2}\,s^{-1}$ was small. The immobilized culture irradiated at 90 μmol photons $m^{-2}\,s^{-1}$ generated only 1.34% more power than the immobilized culture irradiated at 30 μmol photons $m^{-2}\,s^{-1}$. When comparison of maximum power density from suspension and immobilized cultures in Set 1 was made, immobilized cultures were found to generate 9.28% more power than suspension cultures.

Figure 4.5: Maximum Power Density of Suspension and Immobilized Cultures at 30 and 90 µmol photons m^{-2} s^{-1}. Data as means ± S.D. (n=3).

The power output from both suspension and immobilized cultures at 30 μmol photons $m^{-2} s^{-1}$ and from suspension culture at 150 μmol photons $m^{-2} s^{-1}$ increased from Day 0 to Day 8 before decreasing from Day 8 to Day 12. Unlike the other cultures, the power output from immobilized culture at 150 μmol photons $m^{-2} s^{-1}$ dropped from Day 0 to Day 4, increased from Day 4 to Day 8 and decreased again from Day 8 to Day 12. At 30 μmol photons $m^{-2} s^{-1}$, the maximum power output from suspension and immobilized cultures were recorded on Day 8 at 0.267 ± 0.016 mWm^{-2} and 0.308 ± 0.015 mWm^{-2} respectively. These values corresponded with current densities of 5.824 ± 0.525 mAm^{-2} and 5.909 ± 0.819 mAm^{-2} respectively. On the other hand, the highest power density from suspension culture at 150 μmol photons $m^{-2} s^{-1}$ in this second set of experiment was 0.296 ± 0.026 mWm^{-2} on Day 8 with a corresponding current density of 5.289 ± 0.075 mAm^{-2} whereas the maximum power density at 150 μmol photons $m^{-2} s^{-1}$ from immobilized culture in Set 2 was 0.456 ± 0.026 mWm^{-2} on Day 0 with a corresponding current density of 6.378 ± 0.799 mAm^{-2}. The maximum current and power densities of both suspension and immobilized cultures were higher when the BPV devices were irradiated at 150 μmol photons $m^{-2} s^{-1}$ compared to 30 μmol photons $m^{-2} s^{-1}$. Between suspension cultures at 30 μmol photons $m^{-2} s^{-1}$ and 150 μmol photons $m^{-2} s^{-1}$, the maximum power density at 150 μmol photons $m^{-2} s^{-1}$ was 10.86% higher than the maximum power density at 30 μmol photons $m^{-2} s^{-1}$. The maximum power density margin between immobilized cultures at 30 μmol photons $m^{-2} s^{-1}$ and 150 μmol photons $m^{-2} s^{-1}$ was large. The immobilized culture at 150 μmol photons $m^{-2} s^{-1}$ generated 48.05% more power than the immobilized culture at 30 μmol photons $m^{-2} s^{-1}$. When comparison of maximum power density from suspension and immobilized cultures in Set 2 was drawn, immobilized cultures were found to generate 54.04% more power than the free moving cells in suspension cultures.
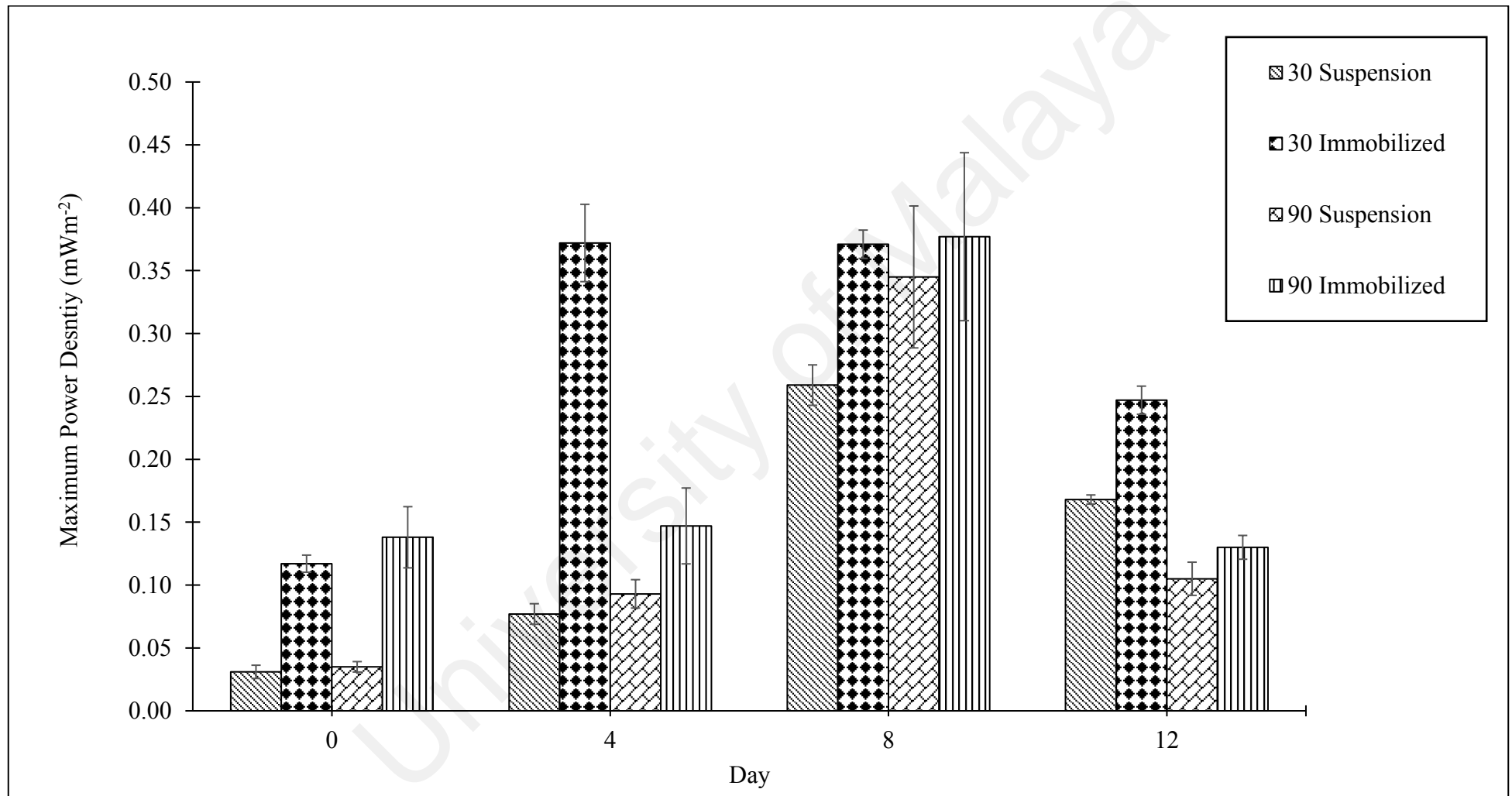
Figure 4.6: Maximum Power Density of Suspension and Immobilized Cultures at 30 and 150 μmol photons m^{-2} s^{-1}. Data as means ± S.D. (n=3).

In the third set of experiment, power output from both suspension and immobilized cultures at 30 μmol photons $m^{-2} s^{-1}$ increased from Day 0 to Day 8 but decreased from Day 8 onwards. However, power output increased from Day 0 until Day 12 at 210 μmol photons $m^{-2} s^{-1}$ for both suspension and immobilized cultures. At 30 μmol photons $m^{-2} s^{-1}$, the maximum power output from suspension and immobilized cultures were recorded on Day 8 at 0.270±0.025 mWm^{-2} with a corresponding current density of 4.953±0.045 mAm^{-2} and 0.378±0.033 mWm^{-2} with a corresponding current density of 5.953±0.063 mAm^{-2} respectively. The maximum power density from suspension culture at 210 μmol photons $m^{-2} s^{-1}$ was 0.098±0.012 mWm^{-2} with a corresponding maximum current density of 3.452±0.214 mAm^{-2}. The maximum power density from immobilized culture at 210 μmol photons $m^{-2} s^{-1}$ was 0.103±0.002 mWm^{-2} with a corresponding maximum current density of 3.422±0.200 mAm^{-2}. The maximum power densities of both the suspension and immobilized cultures at 210 μmol photons $m^{-2} s^{-1}$ were recorded on Day 12. In this set of experiment, the maximum power density and maximum current density for both suspension and immobilized cultures were higher at 30 μmol photons $m^{-2} s^{-1}$. Between suspension cultures at 30 μmol photons $m^{-2} s^{-1}$ and 210 μmol photons $m^{-2} s^{-1}$, the latter produced 175.5% more power than the former. The immobilized culture at 30 μmol photons $m^{-2} s^{-1}$ generated 267% more power than the immobilized culture at 210 μmol photons $m^{-2} s^{-1}$. In terms of percentage, immobilized culture was able to generate 40% more power than suspension culture when the maximum power densities of both cultures were compared.
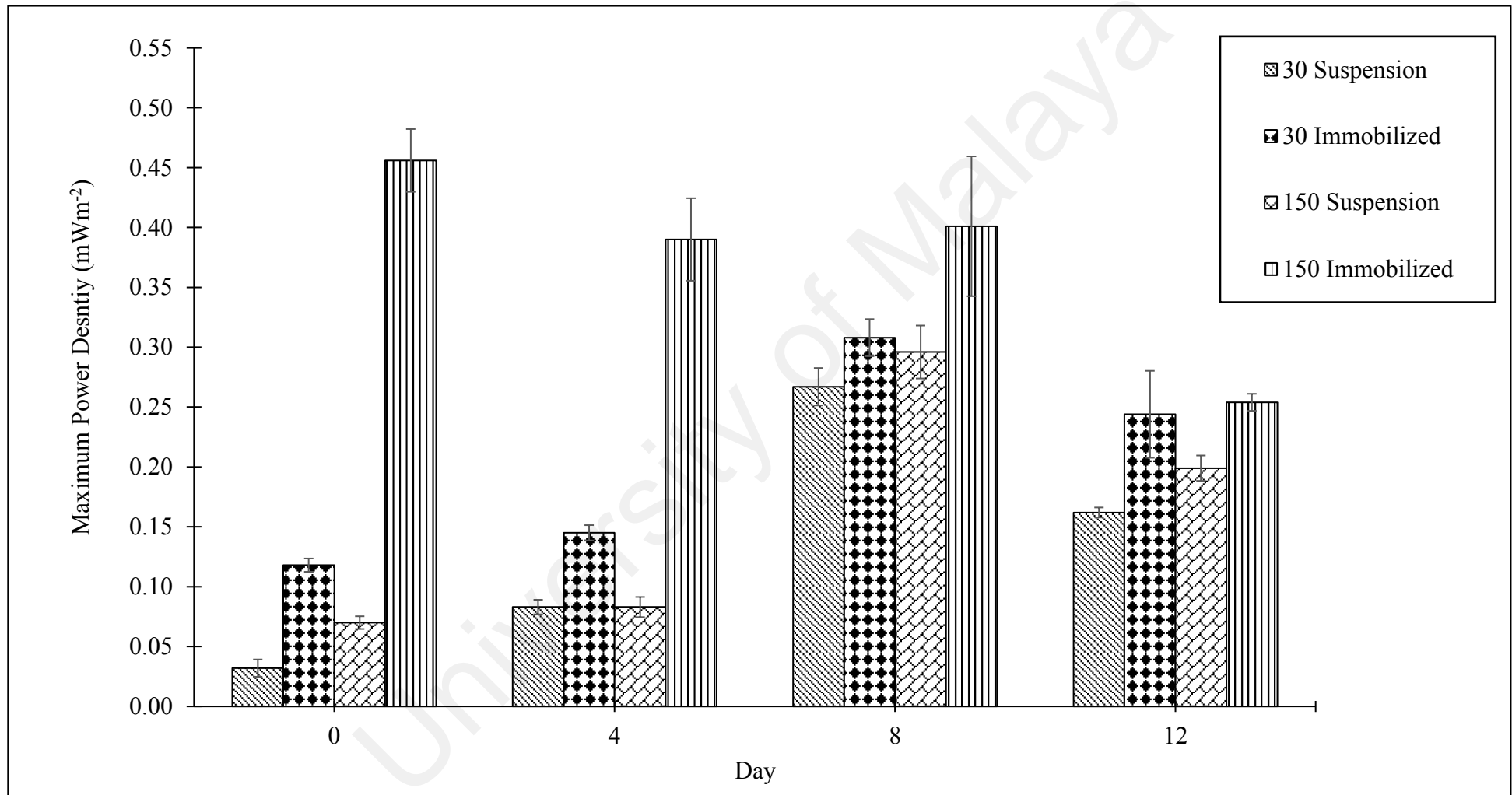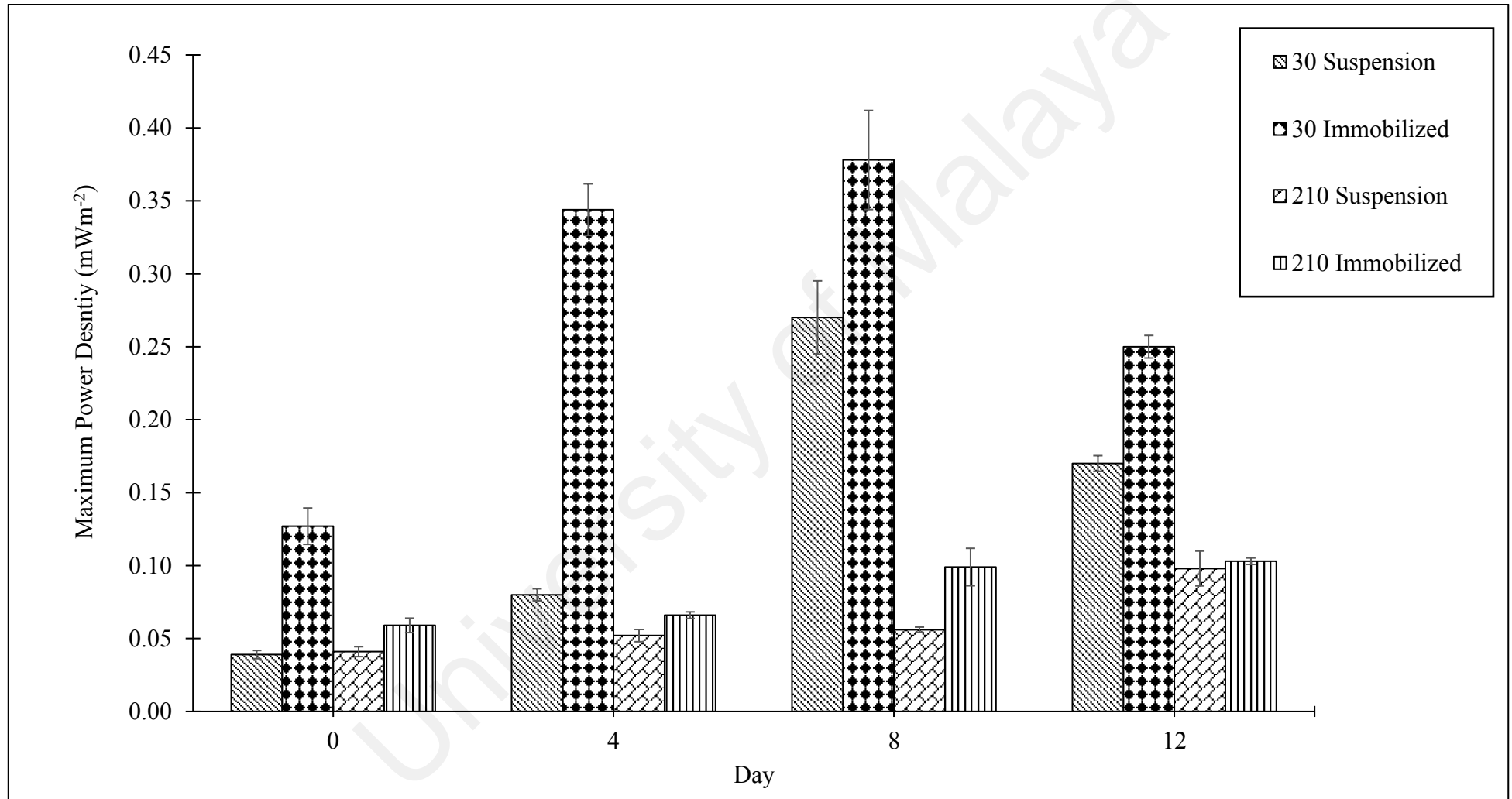
Figure 4.7: Maximum Power Density of Suspension and Immobilized Cultures at 30 and 210 μmol photons m^{-2} s^{-1}. Data as means ± S.D. (n=3).

Based on Figure 4.8 and Figure 4.9, a positive correlation between power output and chl-*a* contents of the cells could be seen as chl-*a* readings in the Control sets as well as at 90 and 150 µmol photons m^{-2} s^{-1} increased with power output from Day 0 to Day 8 before dropping on Day 12, possibly due to nutrient depletion. In Figure 4.10, the chl-*a* readings at 30 and 210 µmol photons m^{-2} s^{-1} were lowest on Day 8 but increased again on Day 12. This phenomenon implied that the cultures in this particular set of experiment were partially photoinhibited and required longer time to adapt to the high irradiance level. The highest chl-*a* values, registered at 90 and 150 µmol photons m^{-2} s^{-1}, corresponded with the highest power outputs in these two sets of experiments. Thus, the optimum range of chl-*a* content for maximum power generation in this particular study was determined to be 13-14 mg L^{-1}. At all irradiance levels investigated in this work, higher power output was observed from immobilized cultures compared to suspension cultures, tallying with the results from the study conducted by Ng *et al.* (2017). These findings are understood as an outcome of minimized liquid-phase mass transfer resistance due to reduced spatial separation between individual algal cells (Ng *et al.*, 2017).

Figure 4.8: Comparison of Maximum Power Density and chl-*a* in Suspension and Immobilized Cultures on Days 0, 4, 8 and 12 at Irradiance Levels of 30 and 90 μmol photons m^{-2} s^{-1}. Data as means ± S.D. (n=3).
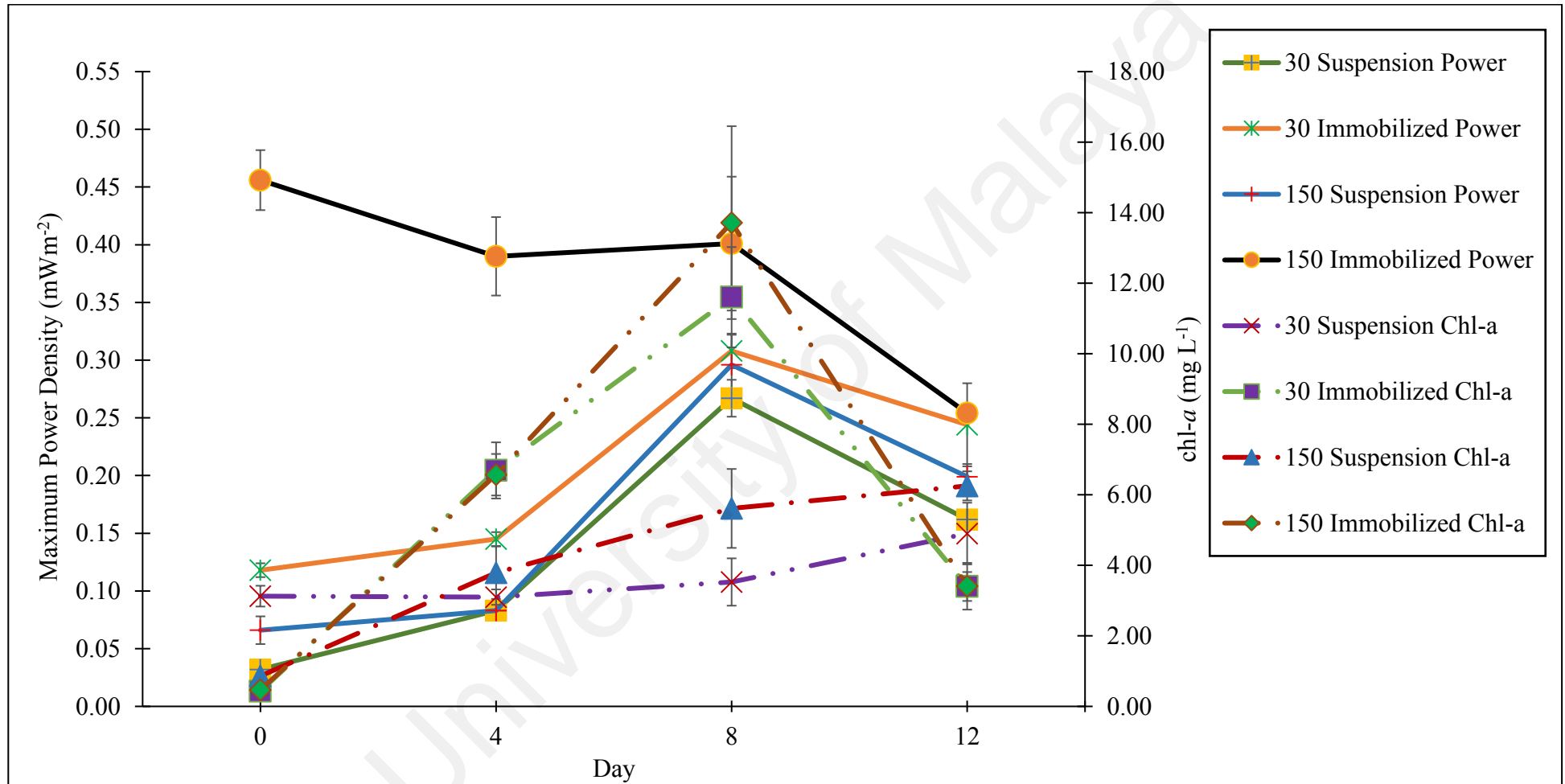
Figure 4.9: Comparison of Maximum Power Density and chl-*a* in Suspension and Immobilized Cultures on Days 0, 4, 8 and 12 at Irradiance Levels of 30 and 150 μmol photons m^{-2} s^{-1}. Data as means ± S.D. (n=3).
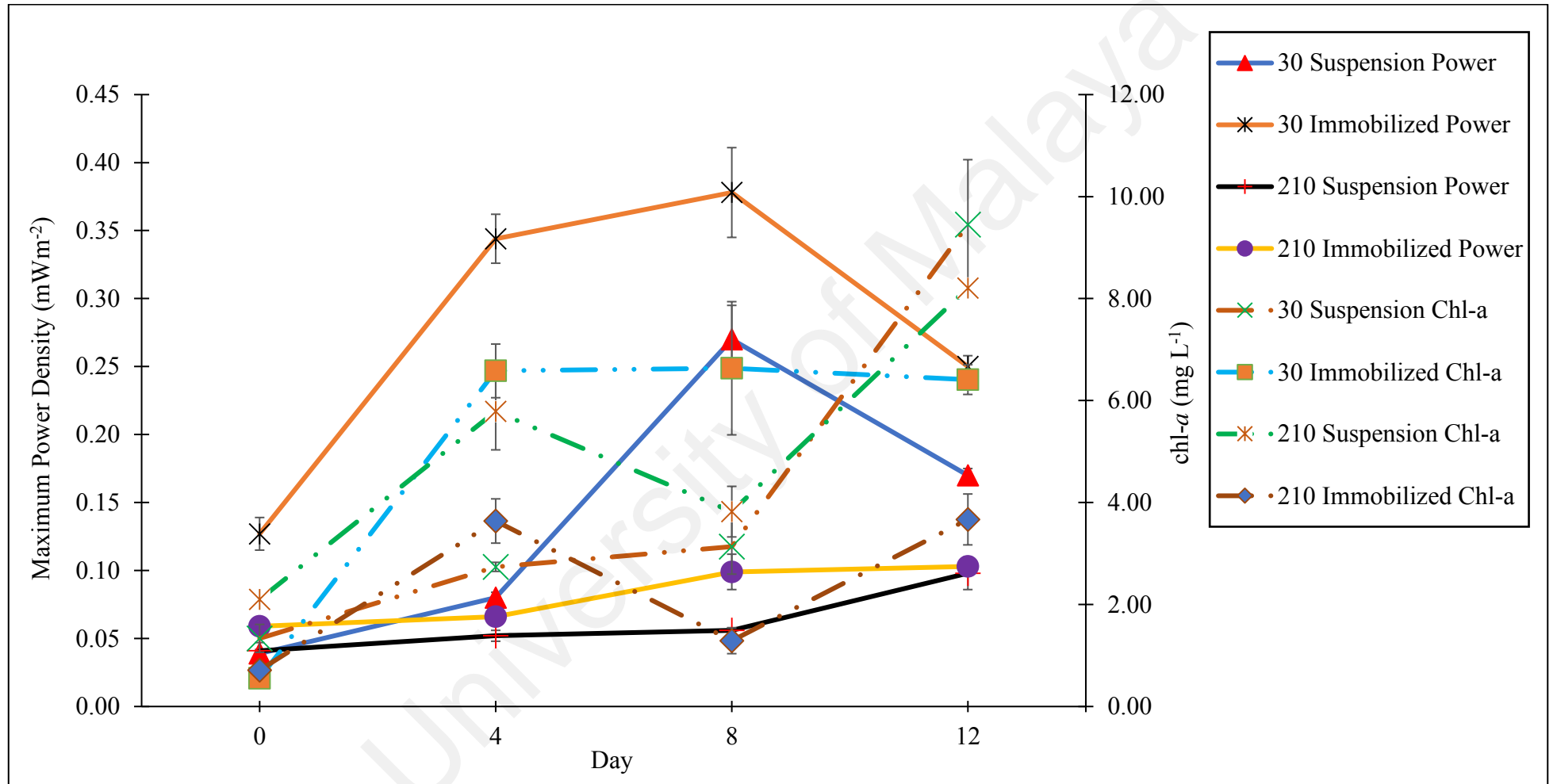
Figure 4.10: Comparison of Maximum Power Density and chl-*a* in Suspension and Immobilized Cultures on Days 0, 4, 8 and 12 at Irradiance Levels of 30 and 210 µmol photons m^{-2} s^{-1}. Data as means ± S.D. (n=3).

After looking at the change in power density and chl-*a* content with respect to time, maximum power density per chl-*a* for each irradiance level was calculated from the power density and chl-*a* content data. Comparisons between all suspension cultures across the four irradiance levels studied pinpointed 23.445±1.586 mWm^{-2} mg chl-*a*$^{-1}$ at 30 µmol photons m^{-2} s^{-1} on Day 8 in Set 1 and 0.701±0.065 mWm^{-2} mg chl-*a*$^{-1}$ at 210 µmol photons m^{-2} s^{-1} on Day 4 as the largest and smallest maximum power density per chl-*a* values respectively. The highest maximum power density per chl-*a* of 326.278±28.033 mWm^{-2} mg chl-*a*$^{-1}$ from immobilized cultures was generated at 150 µmol photons m^{-2} s^{-1} under light condition (Refer to Table 4.2). It was significantly higher ($p < 0.05$) than the maximum power density per chl-*a* at 30 µmol photons m^{-2} s^{-1}, 90 µmol photons m^{-2} s^{-1} and 210 µmol photons m^{-2} s^{-1}. Table 4.3 shows the lowest maximum power density per chl-*a* of 6.500±0.798 mWm^{-2} mg chl-*a*$^{-1}$ from immobilized cultures at 210 µmol photons m^{-2} s^{-1} under light condition. In all 3 sets of experiments, the maximum power density per chl-*a* values of immobilized cultures were higher than the maximum power density per chl-*a* values of suspension cultures when both cultures were compared at the same irradiance level.

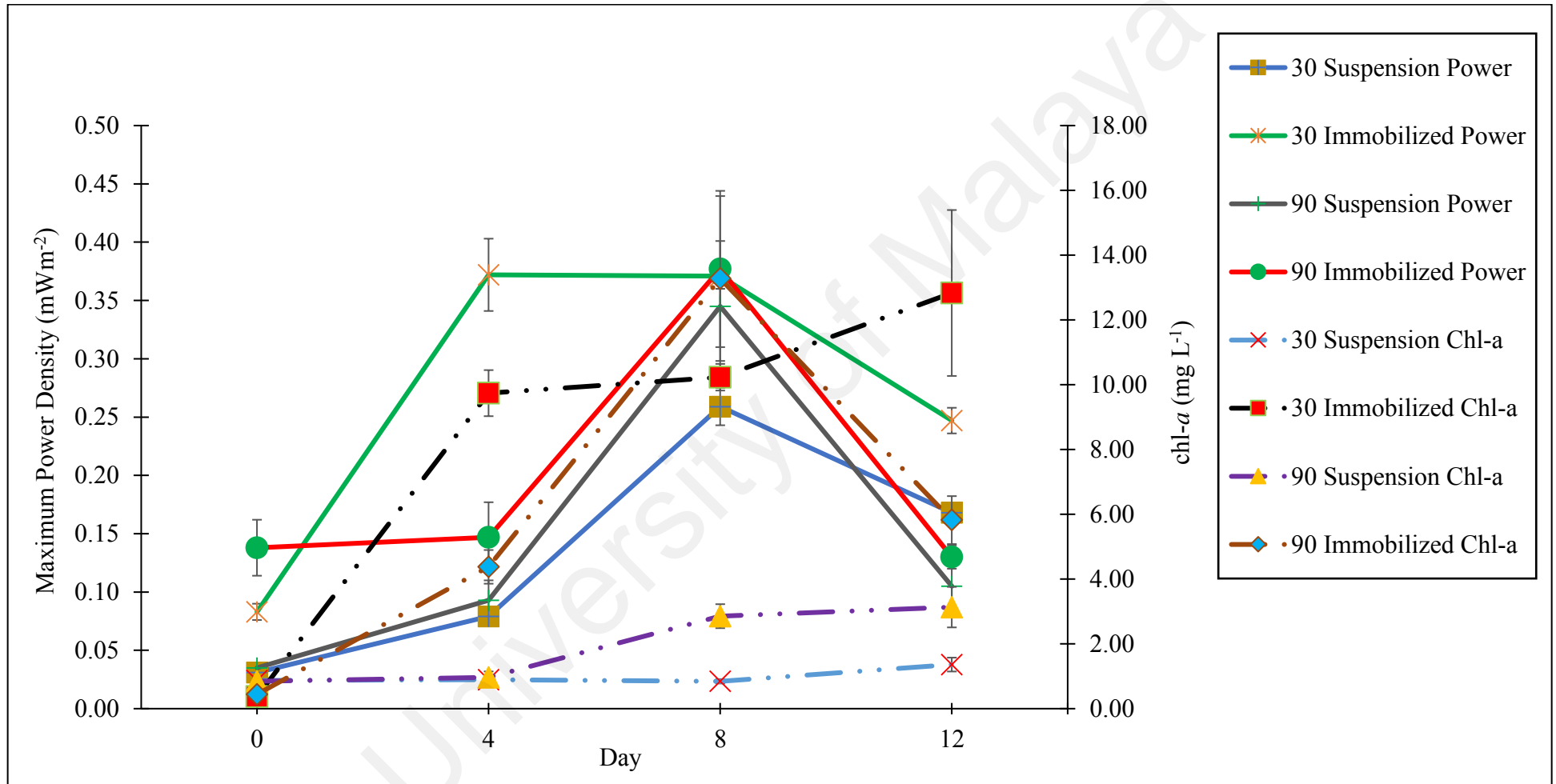**Table 4.1:** Maximum Power Density Per chl-*a* in Light and Dark Conditions for Suspension and Immobilized Cultures at Irradiance Levels of 30 and 90 µmol photons m^{-2} s^{-1}; data as means ± S.D. (n=3). Difference between alphabets indicate significant differences between different irradiance levels (ANOVA, Tukey HSD test, $p < 0.05$).

Day	Maximum Power Density Per Chl-a (mWm^{-2} mg^{-1} chl-*a*)							
	30 Suspension		30 Immobilized		90 Suspension		90 Immobilized	
	Light	Dark	Light	Dark	Light	Dark	Light	Dark
0	2.730±0.509[d]	1.612±0.101[e]	74.173±5.063[b]	60.960±6.415[b]	3.233±0.496[d]	1.900±0.158[e]	104.288±6.404[a]	56.412±6.094[bc]
4	7.028±1.388[cd]	5.660±1.193[de]	12.767±1.139[bcd]	7.494±0.259[de]	8.037±2.391[cd]	6.680±1.508[de]	11.165±1.747[bcd]	9.525±2.109[de]
8	23.445±1.586[bc]	19.055±3.121[cde]	12.101±0.413[bcd]	7.388±0.571[de]	9.364±1.642[bcd]	6.949±0.070[de]	9.944±3.728[bcd]	9.145±1.565[de]
12	9.408±1.588[bcd]	6.326±1.139[de]	6.634±1.566[cd]	4.551±0.674[e]	2.759±0.836[d]	2.162±0.482[e]	7.484±0.441[cd]	5.326±0.280[de]

Table 4.2: Maximum Power Density Per chl-*a* in Light and Dark Conditions for Suspension and Immobilized Cultures at Irradiance Levels of 30 and 150 µmol photons m^{-2} s^{-1}; data as means ± S.D. (n=3). Difference between alphabets indicate significant differences between different irradiance levels (ANOVA, Tukey HSD test, p<0.05).

Day	Maximum Power Density Per chl-*a* (mWm^{-2} mg^{-1} chl-*a*)							
	30 Suspension		**30 Immobilized**		**150 Suspension**		**150 Immobilized**	
	Light	**Dark**	**Light**	**Dark**	**Light**	**Dark**	**Light**	**Dark**
0	0.829±0.102[d]	0.435±0.114[e]	92.318±13.305[b]	54.662±5.313[bc]	6.258±0.411[cd]	4.222±0.430[e]	326.278±28.033[a]	291.265±77.894[a]
4	2.150±0.294[d]	0.878±0.133[e]	7.271±0.932[cd]	4.763±1.391[e]	1.711±0.160[d]	1.291±0.103[e]	19.998±3.607[bcd]	12.180±2.697[de]
8	5.487±1.206[cd]	3.578±0.927[e]	8.963±1.438[bcd]	6.949±1.035[de]	4.163±0.605[d]	2.954±0.862[e]	10.009±2.459[bcd]	6.491±1.696[de]
12	2.520±0.459[d]	1.723±0.548[e]	24.382±6.083[bc]	15.873±1.268[de]	2.464±0.248[d]	2.223±0.389[e]	25.567±5.713[bc]	14.170±2.885[de]

Table 4.3: Maximum Power Density Per chl-*a* in Light and Dark Conditions for Suspension and Immobilized Cultures at Irradiance Levels of 30 and 210 µmol photons m^{-2} s^{-1}; data as means ± S.D. (n=3). Difference between alphabets indicate significant differences between different irradiance levels (ANOVA, Tukey HSD test, p<0.05).

Day	Maximum Power Density Per chl-*a* (mWm^{-2} mg^{-1} chl-*a*)							
	30 Suspension		**30 Immobilized**		**210 Suspension**		**210 Immobilized**	
	Light	**Dark**	**Light**	**Dark**	**Light**	**Dark**	**Light**	**Dark**
0	2.212±0.353[d]	0.896±0.252[e]	77.003±11.604[b]	43.635±4.661[bcd]	1.555±0.136[d]	0.424±0.252[e]	28.084±4.605[b]	22.785±4.119[bcde]
4	2.265±0.177[d]	1.869±0.337[e]	17.527±2.133[bcd]	4.763±1.391[e]	0.701±0.065[d]	0.590±0.161[e]	6.500±0.798[cd]	5.401±0.953[de]
8	6.187±1.384[cd]	1.384±0.912[e]	8.963±1.438[bcd]	6.949±1.035[de]	1.145±0.150[d]	0.954±0.153[e]	26.661±8.035[b]	22.332±5.623[cde]
12	1.309±0.170[d]	0.872±0.129[e]	24.382±6.083[bc]	15.873±1.268[de]	0.917±0.100[d]	0.729±0.062[e]	9.522±1.311[bcd]	8.140±1.009[de]

4.3 Pulse Amplitude Modulation (PAM) Fluorometry

The maximum quantum efficiency of Photosystem II, denoted as the variable Fv/Fm, measures the concentration of open reaction centers in Photosystem II that are actively utilizing the light quanta absorbed for photosynthesis to proceed (Genty *et al.*, 1989). The suspension cultures exhibited a distinctive trait on Day 0; the F_v/F_m values of the suspension cultures in Figure 4.11 were highest on Day 0 at all irradiance levels investigated in this study. The F_v/F_m values of suspension cultures at 30, 90, 150 and 210 µmol photons m^{-2} s^{-1} in all three sets of experiments conducted dropped between Day 0 and Day 4, indicating decline in the physiological state of the algal cells. After Day 4, the increase of F_v/F_m readings at 30 µmol photons m^{-2} s^{-1} in Set 1 and Set 3 as well as at 210 µmol photons m^{-2} s^{-1} implied that the cells irradiated under these conditions were showing signs of improvement in terms of biological functions. At other irradiance levels, the algal cells required a longer period of time to recover to a healthier state with F_v/F_m values increasing only after Day 8. On the other hand, the first 4 days of the experiment seemed to be the adjustment period for immobilized cultures as the F_v/F_m values for all tested irradiance levels in this study were lower on Day 0 compared to Day 4. In general, the F_v/F_m values for immobilized cultures at most irradiance levels experimented began dropping after Day 8 except at 30 µmol photons m^{-2} s^{-1} in the second set of experiment.
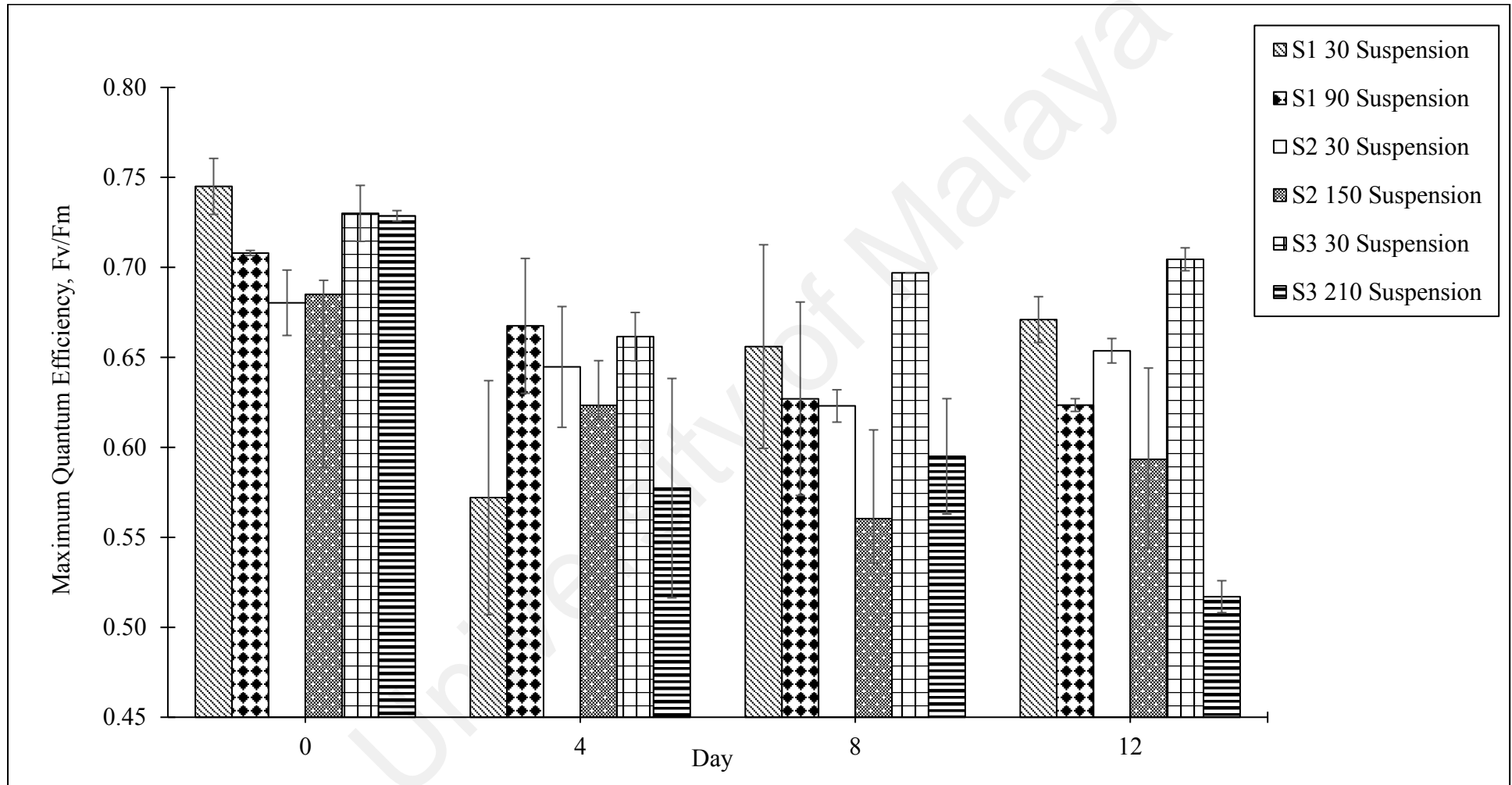
Figure 4.11: Maximum Quantum Efficiency, F_v/F_m Values of Suspension Cultures on Days 0, 4, 8 and 12. Data as means ± S.D. (n=3).
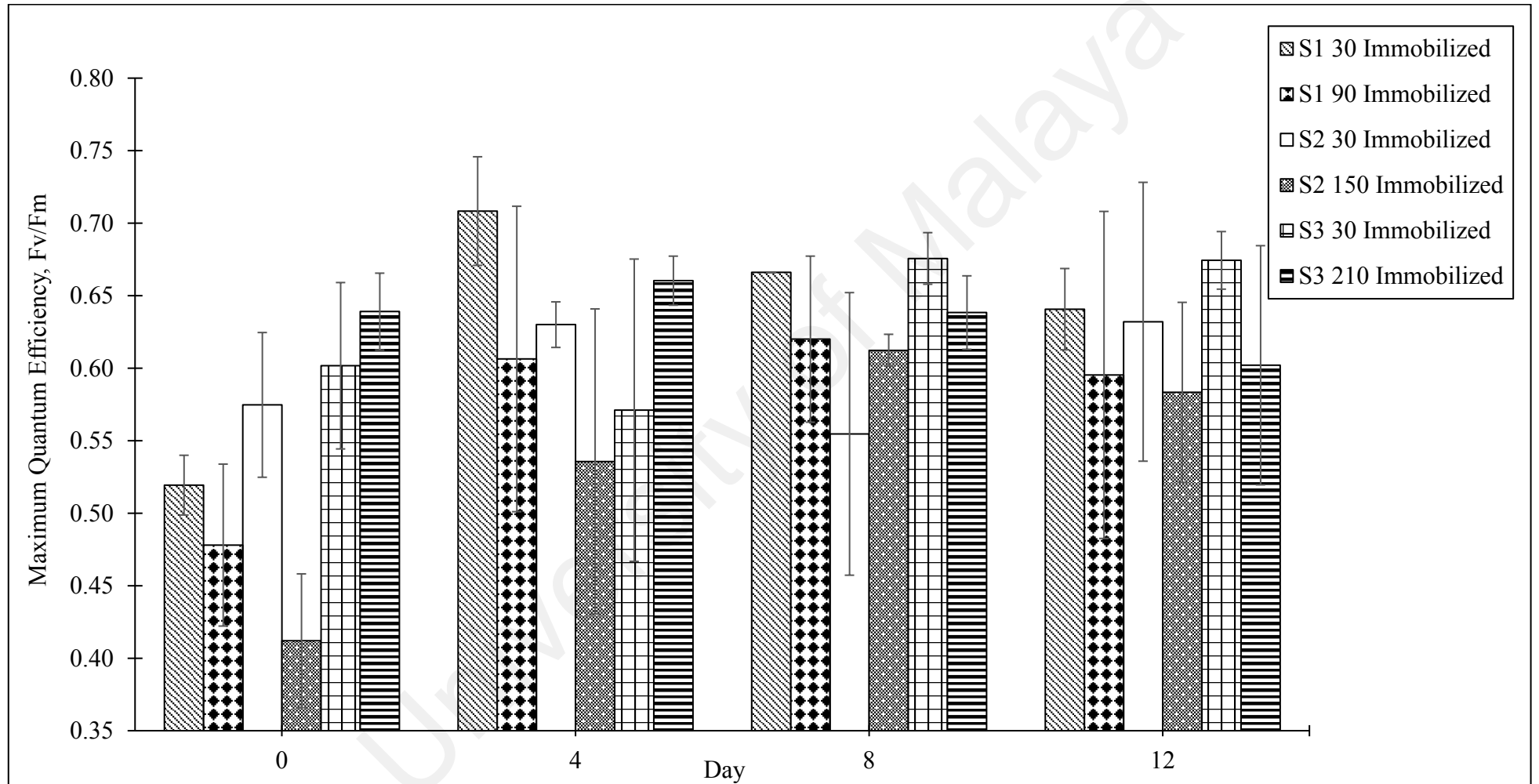
Figure 4.12: Maximum Quantum Efficiency, F_v/F_m Values of Immobilized Cultures on Days 0, 4, 8 and 12. Data as means ± S.D. (n=3).

In the context of Pulse Amplitude Modulation Fluorometer measurements, maximum relative electron transport rate, $rETR_{max}$ represents the rate at which electron is passed along the photosynthetic chain. In suspension cultures, the range of $rETR_{max}$ values fell between 29.048 ± 3.320 µmol electrons m^{-2} s^{-1} and 264.529 ± 11.862 µmol electrons m^{-2} s^{-1}. Both the highest and lowest $rETR_{max}$ values were observed on Day 0 from suspension cultures irradiated under 30 µmol photons m^{-2} s^{-1} in Set 1 and Set 2 respectively. When the $rETR_{max}$ readings were compared across all irradiance levels tested in this study, 90 µmol photons m^{-2} s^{-1} was identified as the irradiance level associated with the highest $rETR_{max}$, followed by 30 µmol photons m^{-2} s^{-1}, 150 µmol photons m^{-2} s^{-1} and 210 µmol photons m^{-2} s^{-1}. The $rETR_{max}$ values significantly decreased (ANOVA, $P < 0.05$) after Day 0 except at 30 µmol photons m^{-2} s^{-1} in Set 2 in which the $rETR_{max}$ value increased until Day 4 of the experiment. Unlike suspension cultures, the lowest and highest $rETR_{max}$ values in immobilized cultures at all irradiance levels experimented in this study were recorded on Day 0 and Day 4 respectively. The $rETR_{max}$ values of the immobilized cultures ranged from 29.048 ± 3.320 µmol electrons m^{-2} s^{-1} and 180.113 ± 4.933 µmol electrons m^{-2} s^{-1}.
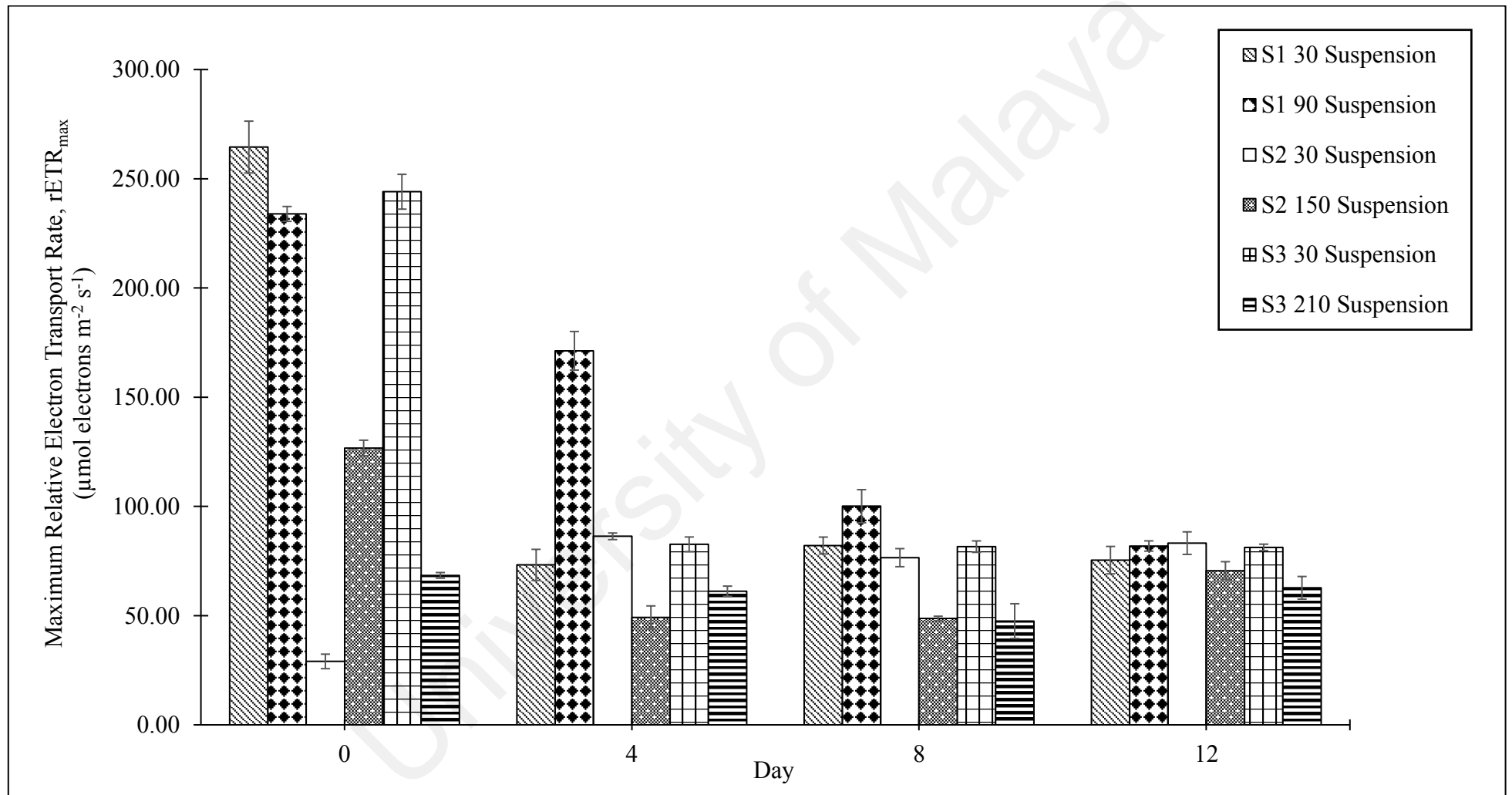
Figure 4.13: Maximum Relative Electron Transport Rate, $rETR_{max}$ of Suspension Cultures on Days 0, 4, 8 and 12. Data as means $\pm$ S.D. (n=3).
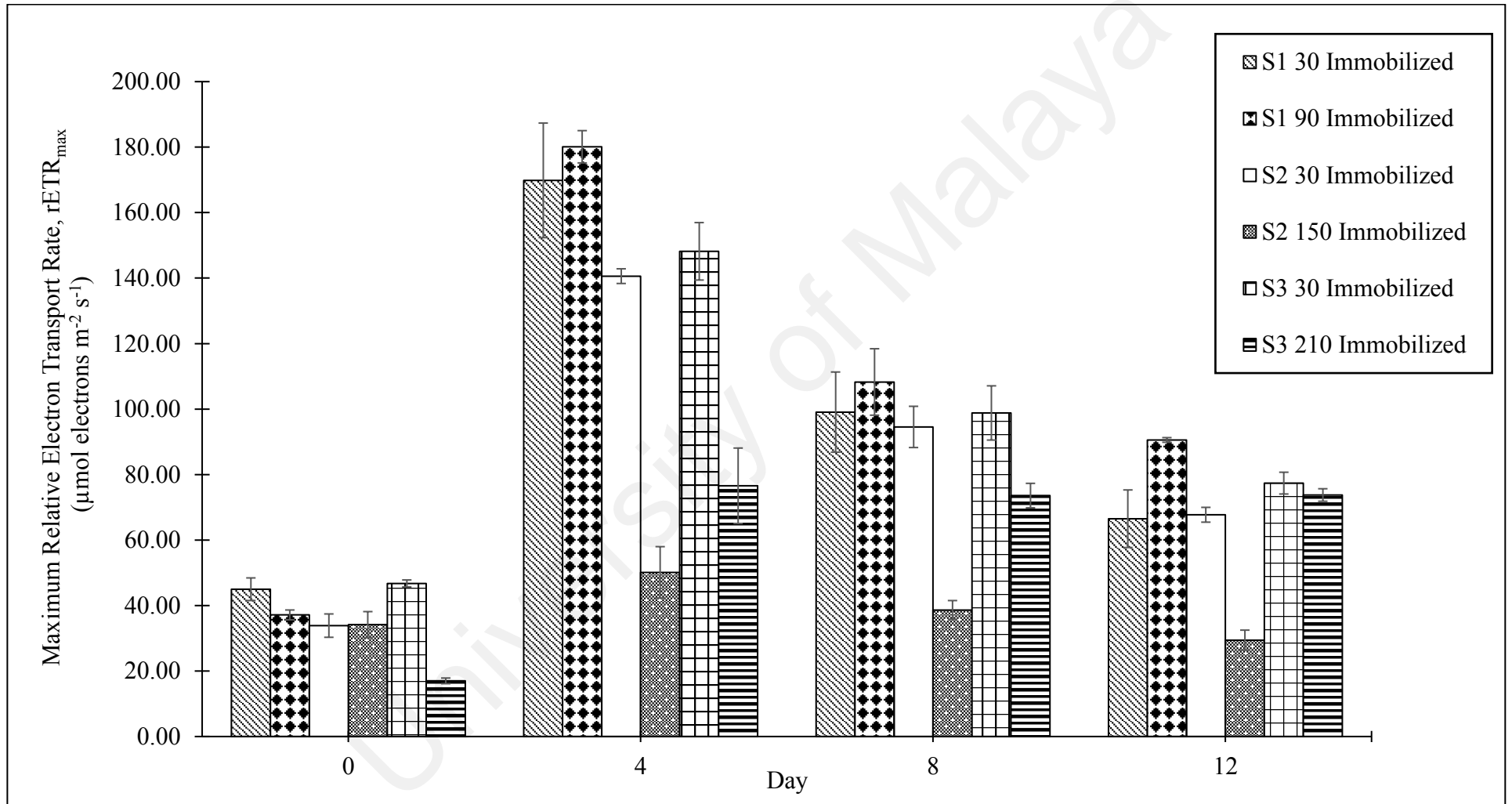
Figure 4.14: Maximum Relative Electron Transport Rate, $rETR_{max}$ of Immobilized Cultures on Days 0, 4, 8 and 12. Data as means ± S.D. (n=3).

The Fv/Fm of the algal cells in the BPV devices when used alone, is a weak representation of the resulting power output of the BPV platform. The light harvesting efficiency of the algal cells is represented by the parameter alpha, α, which translates into a numerical value, the ability of the algal cells to efficiently capture and convert light energy (Malapascua $et\ al.$, 2014). The range of α of suspension cultures was between 0.210±0.004 and 0.769±0.017 with the lowest and highest values measured at 90 µmol photons m^{-2} s^{-1} on Day 4 and 210 µmol photons m^{-2} s^{-1} on Day 8 respectively. When compared with the α of respective control cultures at 30 µmol photons m^{-2} s^{-1}, α for suspension cultures under irradiances of 150 µmol photons m^{-2} s^{-1} and 210 µmol photons m^{-2} s^{-1} were higher on Days 0, 4 and 8 but lower on Day 12. Comparison of α between 30 µmol photons m^{-2} s^{-1} and 90 µmol photons m^{-2} s^{-1} showed otherwise. The α at 90 µmol photons m^{-2} s^{-1} was lower than the α at 30 µmol photons m^{-2} s^{-1} on all measurement days except on Day 0. On the other hand, the range of α for immobilized cultures was between 0.179±0.007 and 0.843±0.033 in which both the highest and lowest values were recorded at 210 µmol photons m^{-2} s^{-1} on Day 0 and Day 8 respectively. The high α values at 210 µmol photons m^{-2} s^{-1} showed that immobilized cultures were capable of capturing light with higher efficiency at high irradiance compared to lower irradiance levels of 30 µmol photons m^{-2} s^{-1}, 90 µmol photons m^{-2} s^{-1} and 150 µmol photons m^{-2} s^{-1}.
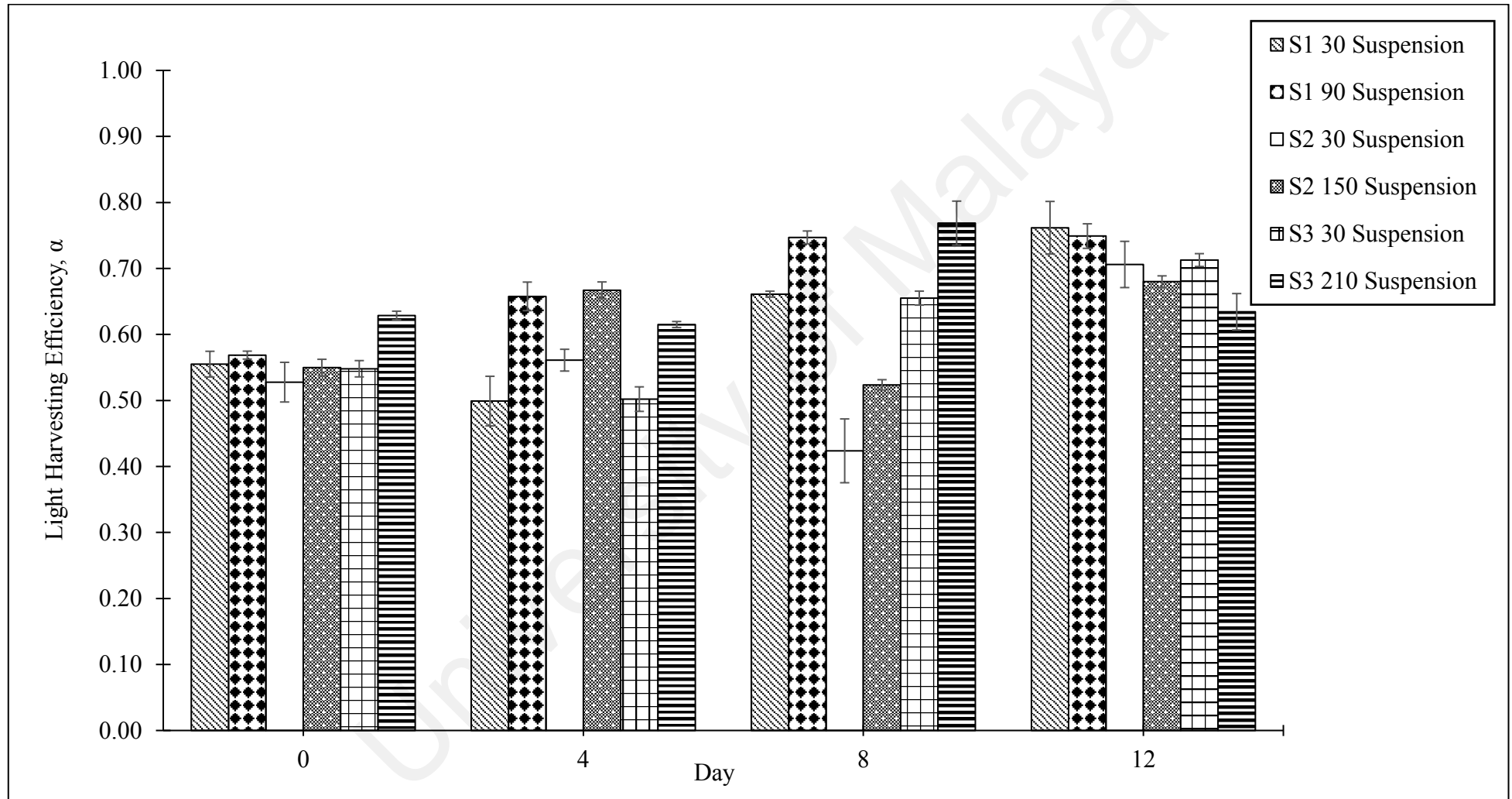
Figure 4.15: Light Harvesting Efficiency, α of Suspension Cultures on Days 0, 4, 8 and 12. Data as means ± S.D. (n=3).
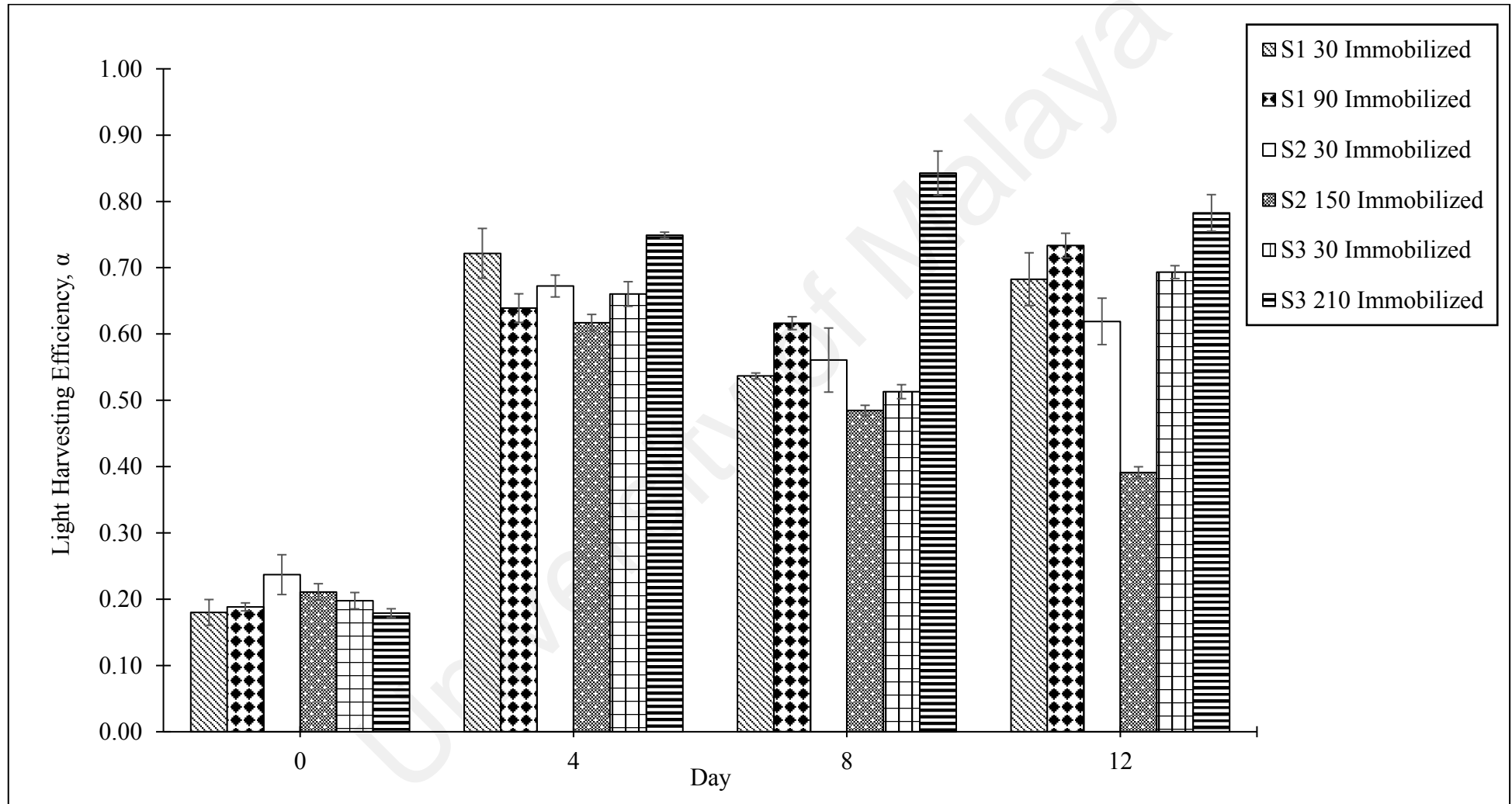
Figure 4.16: Light Harvesting Efficiency, α of Immobilized Cultures on Days 0, 4, 8 and 12. Data as means ± S.D. (n=3).

Photoadaptive index, E_k defines the optimum irradiance level for photosynthetic activity to occur. The E_k values for suspension cultures ranged from 57.137 ± 3.758 μmol photons m^{-2} s^{-1} to 476.539 ± 17.709 μmol photons m^{-2} s^{-1} with both the highest and lowest E_k values measured at 30 μmol photons m^{-2} s^{-1} on Day 0 of Set 2 and Set 1 respectively. In suspension cultures, the E_k values for 90 μmol photons m^{-2} s^{-1} were higher than the E_k values for 30 μmol photons m^{-2} s^{-1} but the E_k values for suspension cultures receiving 150 μmol photons m^{-2} s^{-1} and 210 μmol photons m^{-2} s^{-1} of light were lower than the E_k values for 30 μmol photons m^{-2} s^{-1}. The E_k values for immobilized cultures ranged from 80.004 ± 4.572 μmol photons m^{-2} s^{-1} to 282.163 ± 14.924 μmol photons m^{-2} s^{-1}. The highest and lowest E_k readings for immobilized cultures were taken at the irradiance levels of 90 μmol photons m^{-2} s^{-1} on Day 4 and 150 μmol photons m^{-2} s^{-1} on Day 8 respectively. Immobilized cultures at 30 μmol photons m^{-2} s^{-1} for Set 2 and Set 3 produced higher E_k values than immobilized cultures at 150 μmol photons m^{-2} s^{-1} and 210 μmol photons m^{-2} s^{-1}, thus suggesting that immobilized cultures at 30 μmol photons m^{-2} s^{-1} were able to adapt to the light exposed better than the cultures at the other two irradiance levels.
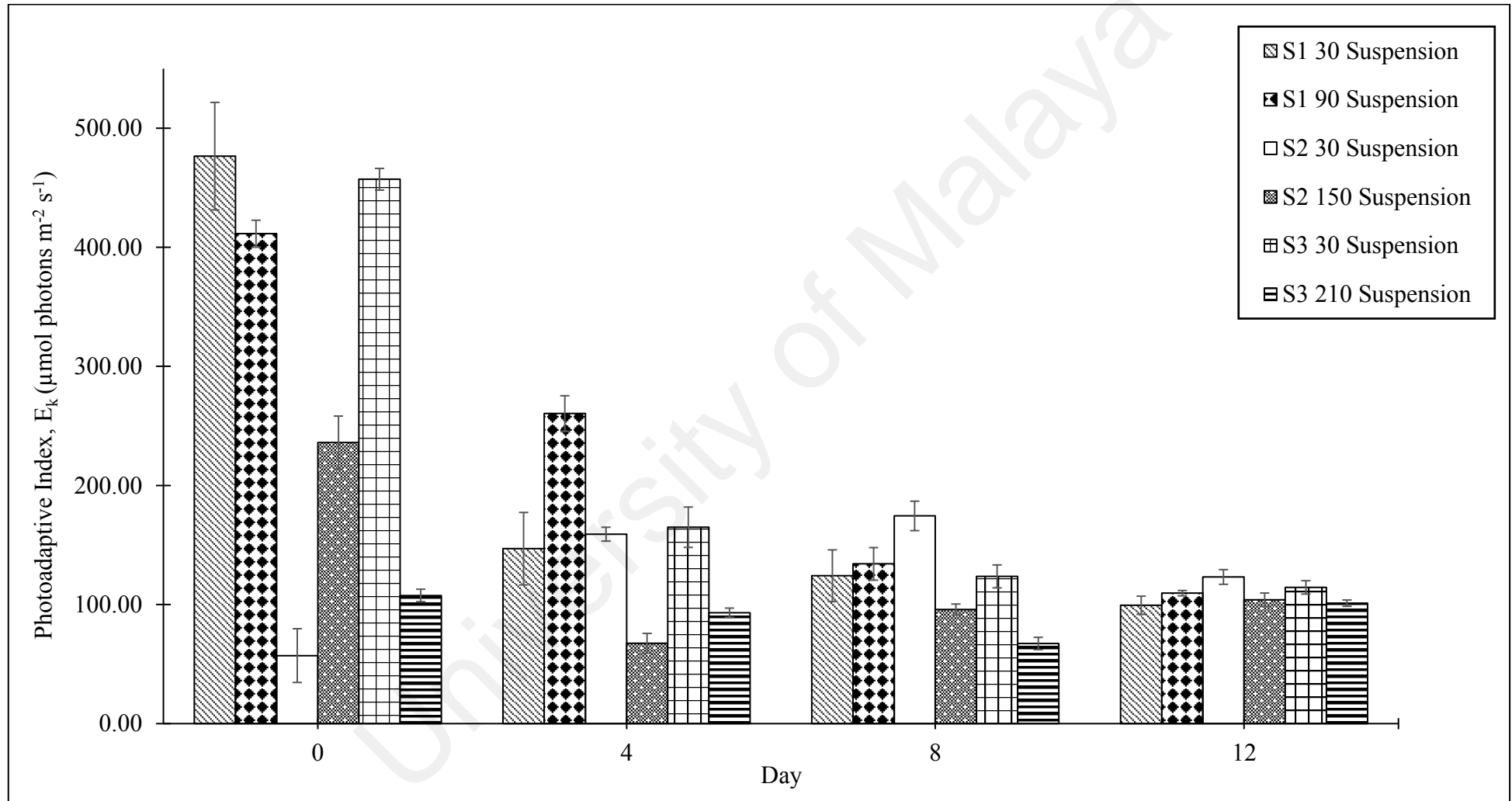
Figure 4.17: Photoadaptive Index, E_k of Suspension Cultures at Days 0, 4, 8 and 12. Data as means ± S.D. (n=3).
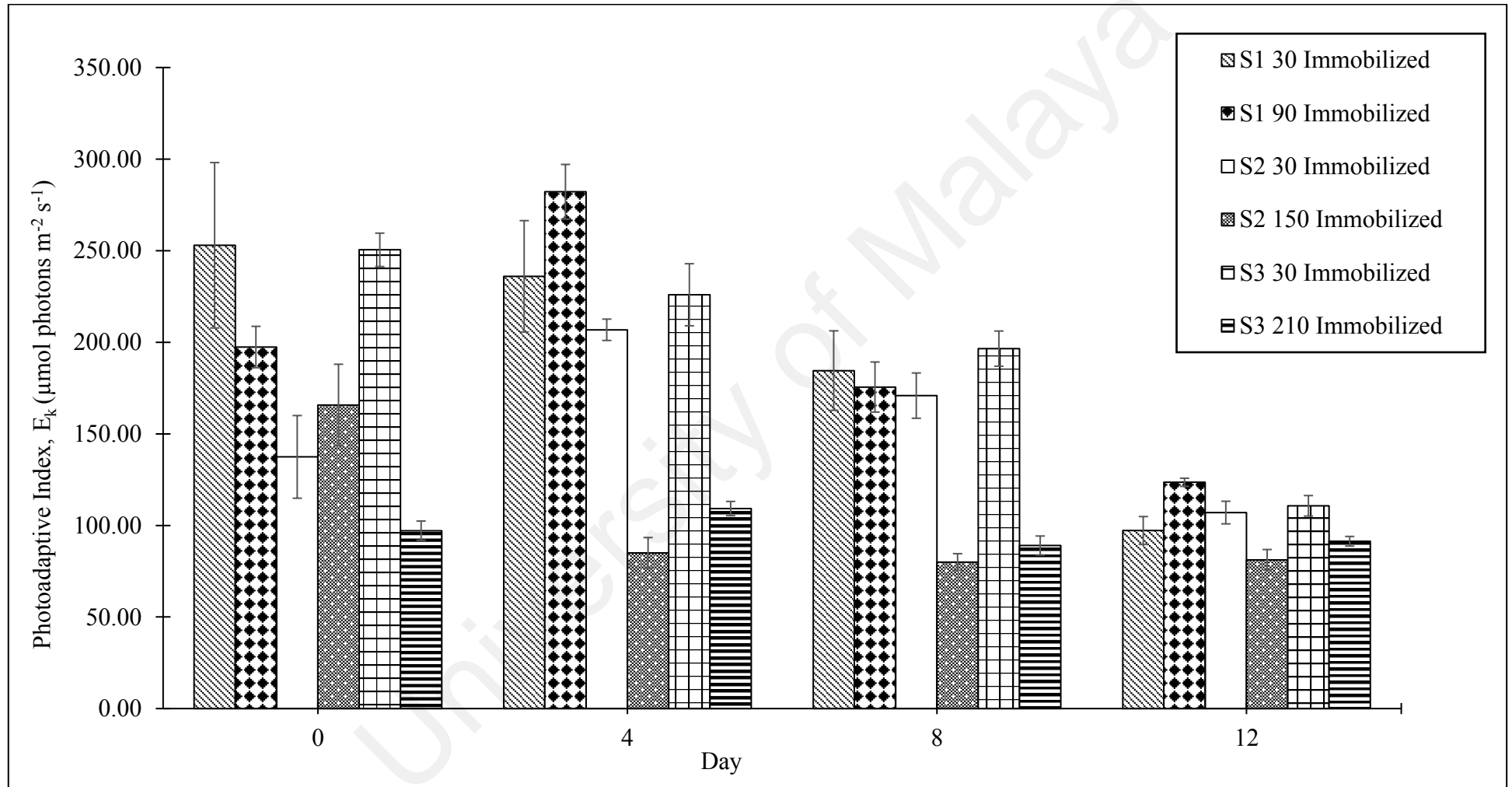
Figure 4.18: Photoadaptive Index, E_k of Immobilized Cultures at Days 0, 4, 8 and 12. Data as means ± S.D. (n=3).

Non-Photochemical Quenching (NPQ) indicates stress in algal cells by enumerating excitation energy dissipated from Chl in PSII. In suspension cultures (Refer to Figure 4.19), the NPQ values ranged between 0.04 and 0.20 at all irradiance levels except at 30 μmol photons m^{-2} s^{-1} in Set 2 where the highest NPQ value was recorded as 0.340. On the other hand, the NPQ trend in immobilized cultures (Figure 4.20) was consistent but the NPQ values were significantly higher (P<0.05) at 150 μmol photons m^{-2} s^{-1} and 210 μmol photons m^{-2} s^{-1}. At these high irradiance levels, high NPQ values were expected as the excess energy was effectively downregulated through elimination of energy in terms of heat.
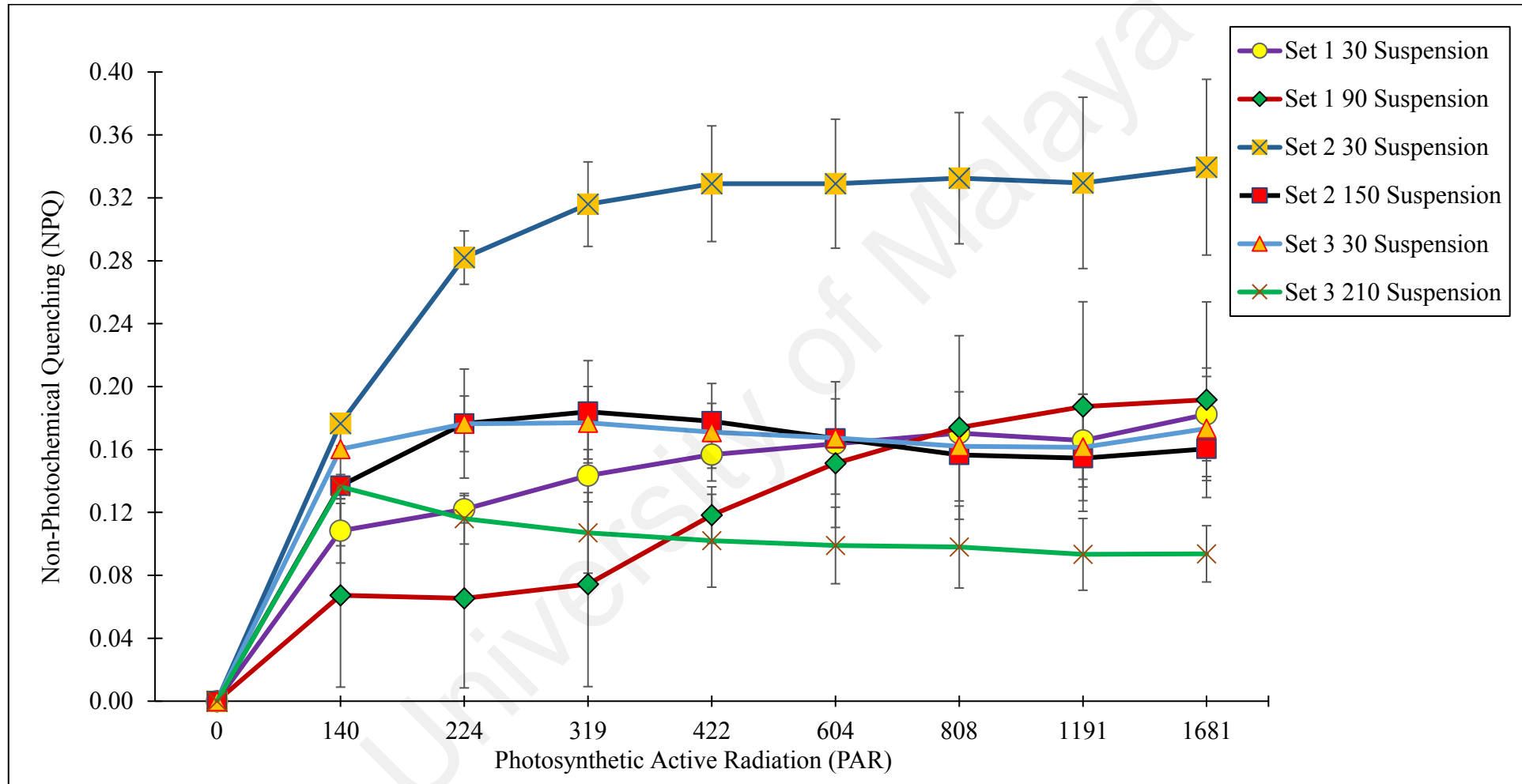
Figure 4.19: Non-Photochemical Quenching, NPQ Values of Suspension Cultures in Algal BPV Devices that Generate Highest Power Output at Irradiance Levels of 30, 90, 150 and 210 µmol photons $m^{-2} s^{-1}$. Data as means ± S.D. (n=3).
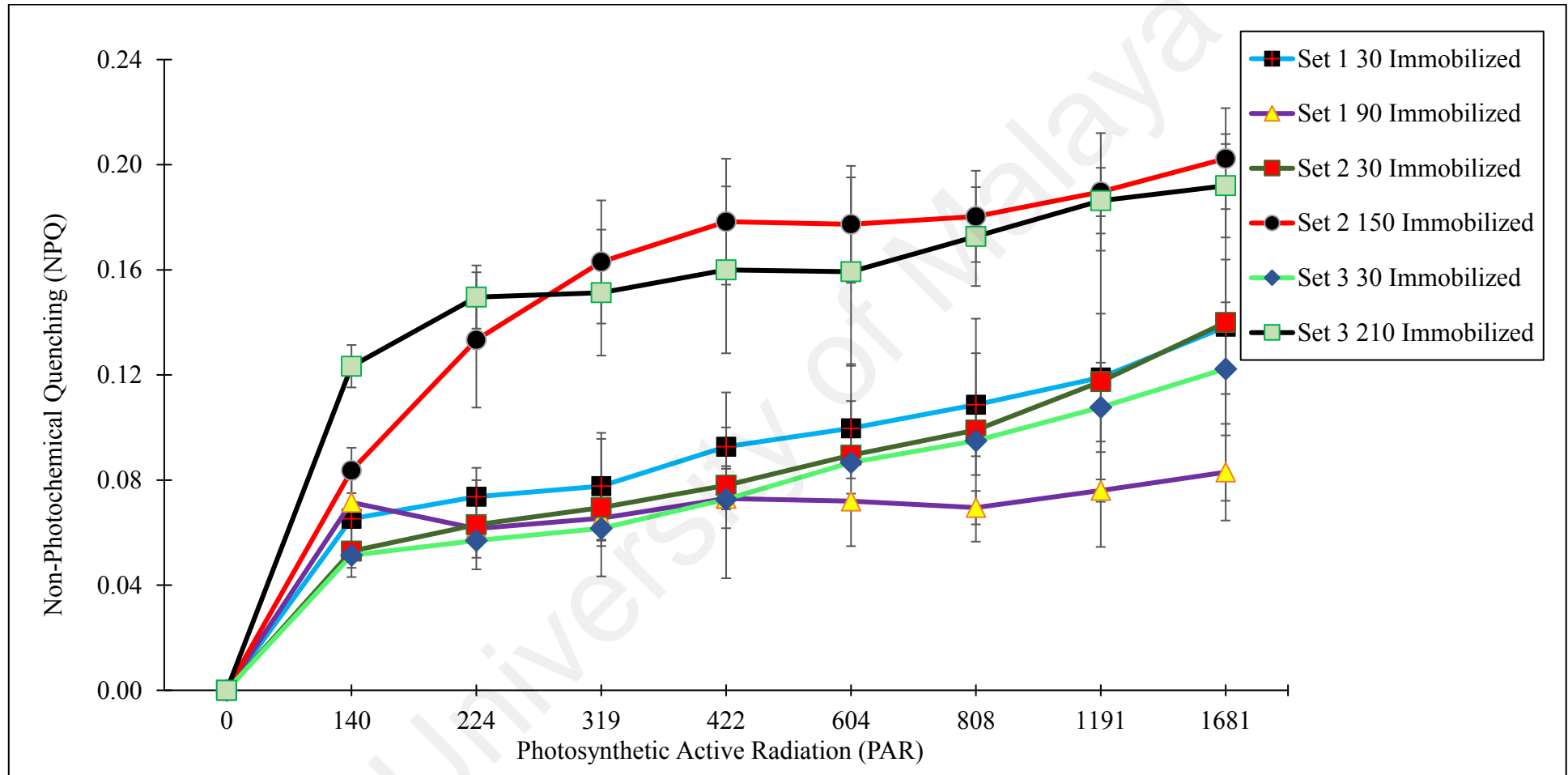
Figure 4.20: Non-Photochemical Quenching, NPQ Values of Immobilized Cultures in BPV Devices that Generate Highest Power Output at Irradiance Levels of 30, 90, 150 and 210 µmol photons m^{-2} s^{-1}. Data as means ± S.D. (n=3).

Carotenoids act as another line of defense against photodamage and thus, complements NPQ and F_v/F_m in interpreting photo-induced stress in the algal cells. In Set 1, the highest and lowest carotenoids readings of 5.739 mg/L and 0.193 mg/L was found at 90 µmol photons m^{-2} s^{-1} on Day 8 and at 30 µmol photons m^{-2} s^{-1} on Day 0 respectively. Both the highest and lowest carotenoids values in Set 1 were found in immobilized cultures. By comparison, the statistical difference between carotenoids level at 30 µmol photons m^{-2} s^{-1} and 90 µmol photons m^{-2} s^{-1} was found to be significant (ANOVA, $P<0.05$). In Set 2, the highest carotenoids reading was recorded in immobilized cultures at 6.030 mg/L on Day 8 but the lowest reading was measured as 0.193 mg/L in immobilized cultures at 30 µmol photons m^{-2} s^{-1} on Day 4. Unlike Set 1 and Set 2, the highest carotenoids level in Set 3 was found in suspension cultures at 30 µmol photons m^{-2} s^{-1} on Day 12. At both 30 µmol photons m^{-2} s^{-1} and 210 µmol photons m^{-2} s^{-1}, the carotenoids levels for both suspension and immobilized cultures were highest on Day 12, thus indicating that the algal cells were exposed to light stress after prolonged exposure to high irradiance.
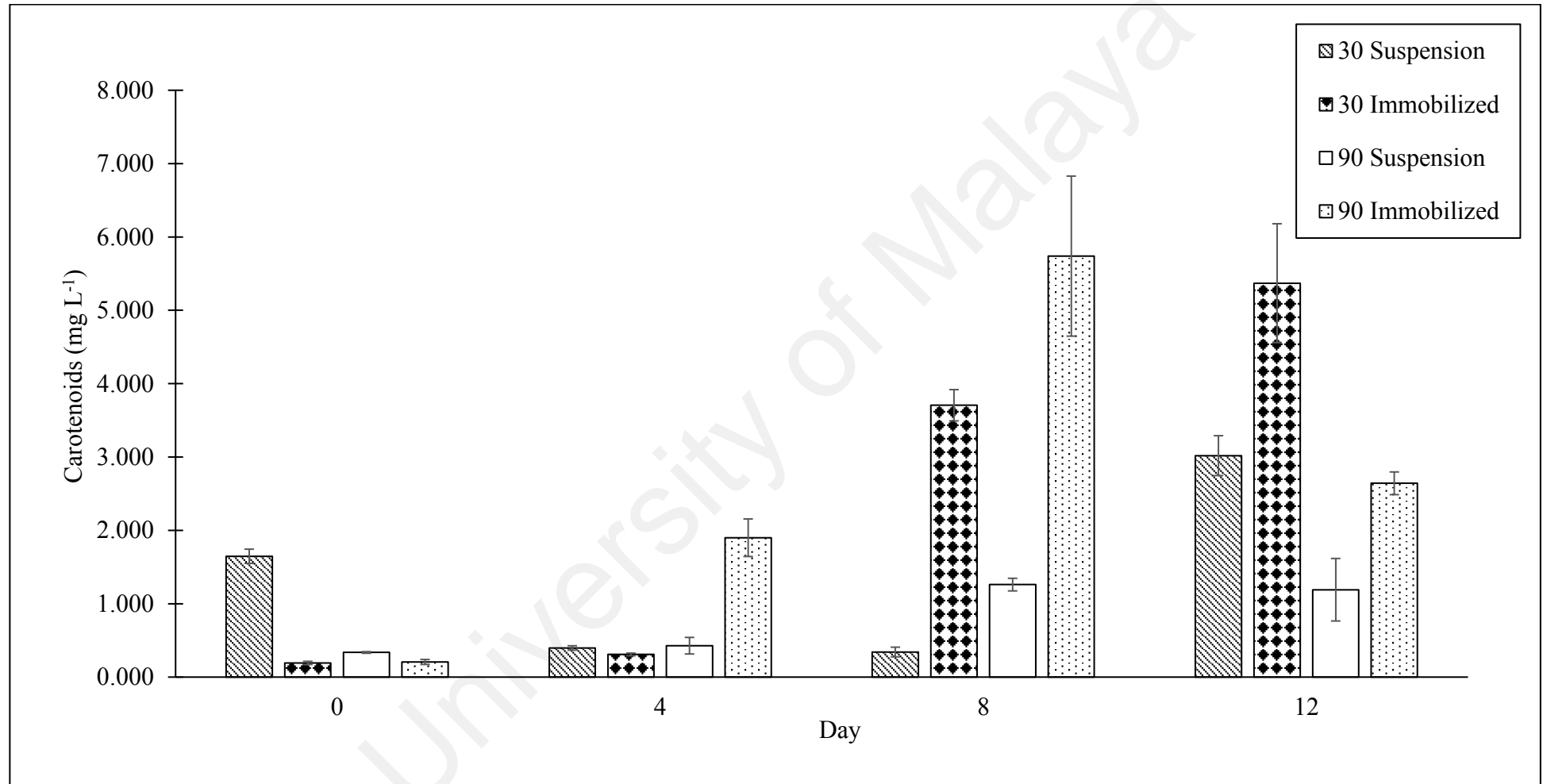
Figure 4.21: Carotenoids Content of Suspension and Immobilized Cultures at 30 and 90 μmol photons $m^{-2} s^{-1}$ on Days 0, 4, 8 and 12. Data as means ± S.D. (n=3).
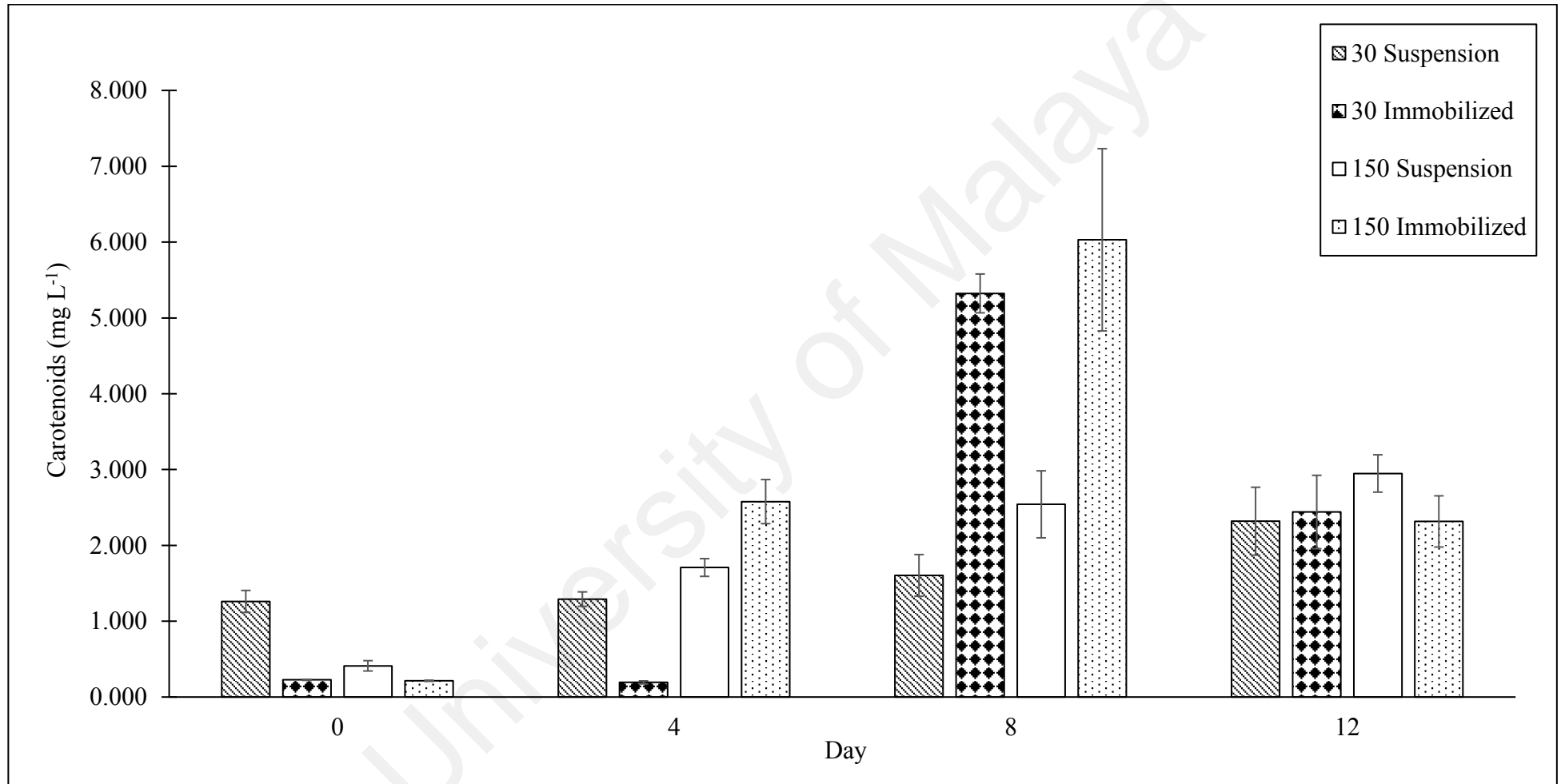
Figure 4.22: Carotenoids Content of Suspension and Immobilized Cultures at 30 and 150 µmol photons $m^{-2} s^{-1}$ in Set 2 on Days 0, 4, 8 and 12. Data as means ± S.D. (n=3).
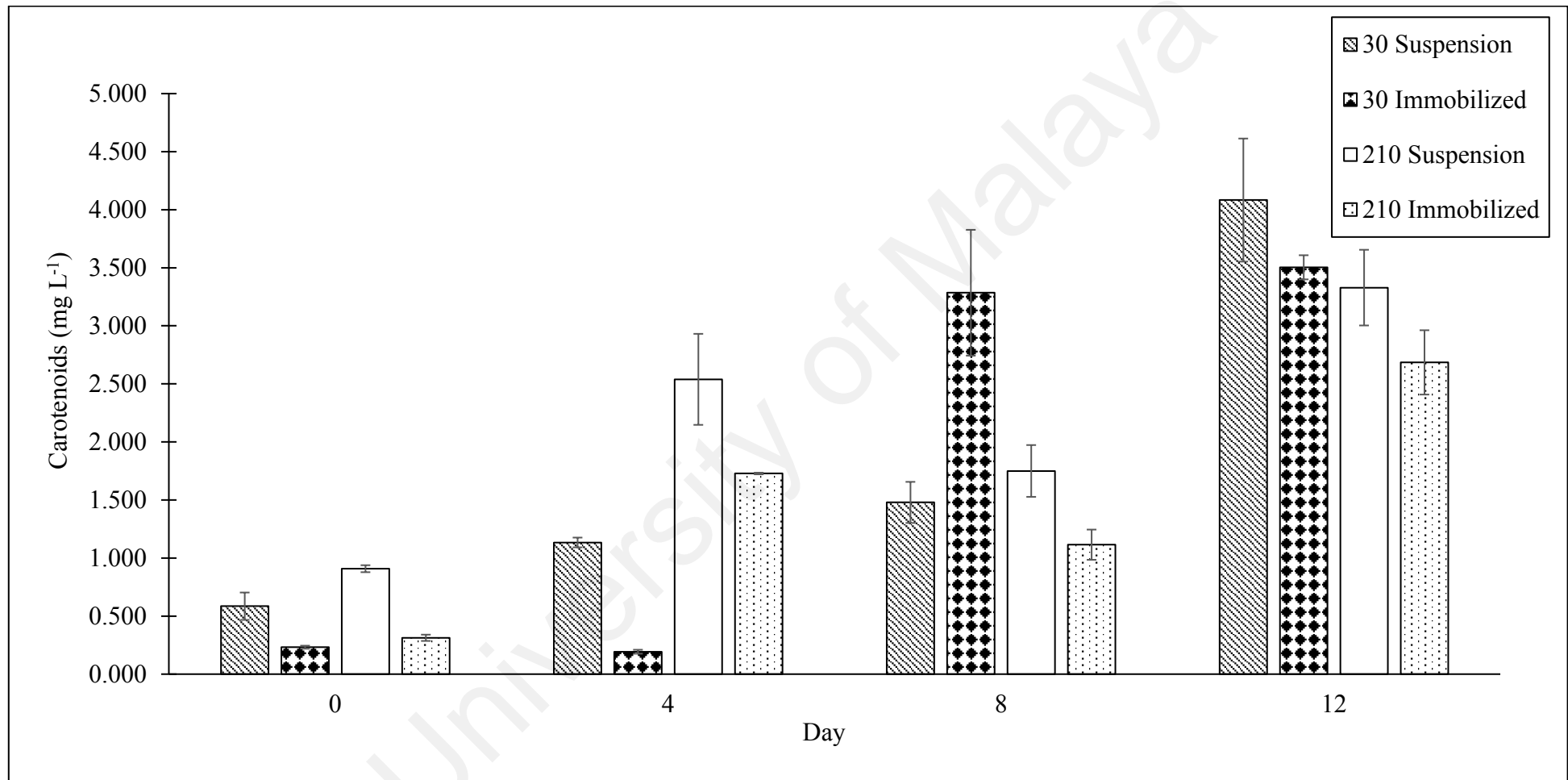
Figure 4.23: Carotenoids Content of Suspension and Immobilized Cultures at 30 and 210 μmol photons $m^{-2} s^{-1}$ in Set 2 on Days 0, 4, 8 and 12. Data as means ± S.D. (n=3).

CHAPTER 5: DISCUSSION

5.1 Effect of Different Irradiance Levels on Growth and Specific Growth Rate

In this study, algal growth was mainly influenced by the irradiance levels that the cultures were exposed to. The biomass and specific growth rate (SGR) of the suspension cultures increased with increasing irradiance except when irradiance was raised to 210 μmol photons m^{-2}s^{-1}. Increasing amount of light below saturating light limit for the algal cells increases cell metabolism in terms of ATP and NADPH production for growth (Mettler *et al.*, 2014). Thus, increasing cell metabolism in response to higher irradiance may have stimulated active cell growth. However, at the highest irradiance of 210 μmol photons m^{-2}s^{-1}, the decrease in SGR indicated possible stress on the cells. At all irradiance levels except for 210 μmol photons m^{-2}s^{-1}, the immobilized cultures had higher biomass. The higher growth rates of immobilized cultures at high irradiance resulted from effective light utilization by amassed cells within a specific unit area (Kosourov & Seibert, 2008). The increasing cell density in response to effective light utilization became a limiting factor once the area occupied by these cells became too crowded for the growing cell population. The compact cell colonies cramped together to induce mutual cell shading which eventually slowed down the growth rate of the cultures. The chl-*a* content of all immobilized cultures on Day 4 was significantly higher than Day 0 ($p<0.05$), signifying that the algal cells had multiplied fast within the first 4 days before conditions became unsuitable for the algal cells, for example due to depleting nutrients. The immobilized cultures however, did not exhibit a positive linear relationship between irradiance and SGR.

5.2 Effect of Different Irradiance Levels on Power Output

In the process of determining power output from the BPV devices, the open circuit potential (OCP) was first measured to determine the electric potential between the two

terminals (anode and cathode) without current flowing through the circuit. Through the resistance stepping technique in which 10 different external resistance loads were applied to the BPV devices before the potential differences between the anode and the cathode were measured with a multimeter, power curves representing power density as a function of current density were generated to pinpoint the maximum power density that the devices were able to generate. In this study, the highest power outputs from suspension culture and immobilized culture were produced under illuminations of 90 μmol photons m^{-2} s^{-1} and 150 μmol photons m^{-2} s^{-1} respectively, thus signifying that illumination of BPV devices loaded with algal cultures at higher irradiance enhanced power generation to a certain extent before power output sank as the effect of photo-induced stress set in. Photo-induced stress signifies deterioration in algal physiology due to absorbance of light exceeding the saturation point for maximum photosynthetic activity. Once excessive light inflicts oxidative damage on the reaction centers of PSII, electron transfer along the electron transport chain is obstructed (Han *et al.*, 2000), dampening power output from the algal BPV devices.

In a recent study conducted by Ng *et al.* (2017), the maximum power density obtained from immobilized culture irradiated with 30 μmol photons m^{-2} s^{-1} of light was 0.289$\pm$0.004 mWm^{-2}. Since the maximum power density of immobilized culture at 90 μmol photons m^{-2} s^{-1} was 0.377$\pm$0.067 mWm^{-2}, comparison with the findings of Ng and collaborators (2017) translates it into a 30.45% increase in power density. The maximum power output at 90 μmol photons m^{-2} s^{-1} is explainable with a relatively high F_v/F_m of 0.620$\pm$0.057 and Chl-a content of 13.278$\pm$2.545 mg chl-*a* L^{-1}. Young and Beardall (2003) justified the improvement in F_v/F_m as a result of increasing maximal fluorescence emission, F_m which signals growing effectiveness in capturing of light and energy transmittance to PSII. Since the F_v/F_m value of the algal cells at 90 μmol photons m^{-2} s^{-1}

was higher than 0.6, high power output from the BPV devices signified that electron channeling to PSII was effectively carried out, commensurate with the large amount of chlorophyll entrapped within the alginate film. Once the threshold amount of chl-*a* for peak power generation under this specific light condition was hit, chl-*a* values began plummeting. The reason for the extensive drop in chl-*a* from 13.278 ± 2.545 mg chl-*a* L^{-1} on Day 8 to 5.821 ± 0.740 mg chl-*a* L^{-1} on Day 12 was likely as explained by Guedes *et al.* (2010), which was unnecessary need for supplementation of cellular chlorophyll when multiplying microalgal cells had already captured adequate amount of light energy.

The highest power density from immobilized culture at 150 μmol photons $m^{-2}s^{-1}$ was 0.456 ± 0.026 mWm^{-2}, which was 57.79% higher than the power density reported by Ng *et al.* (2017) and 48.05% higher than the highest power density generated by immobilized culture at 30 μmol photons $m^{-2}s^{-1}$ in this study. Despite so, lower F_v/F_m, $rETR_{max}$ and α values of the immobilized culture indicated lowered efficiency in both the light capturing and linear electron transport mechanisms of the algal cells. Thus, the high power output at 150 μmol photons $m^{-2}s^{-1}$ was more likely to be concomitant of uniform presence of carboxylic molecules in alginate that established stronger connection for electron transfer between the algal cells and the ITO anode surface (Ng *et al.*, 2017), on top of an effective NPQ mechanism that protects algal cells from potential photo-induced damages. Li *et al.* (2012) explained that carboxylic groups in sodium alginate allow development of more binder-bonds for electrode materials, thus building strong contact between the electrode, electrolyte and electron donor. Torres *et al.* (2010), on the other hand, enunciated electron attraction towards the anode surface as a result of migration forces from agglomerated electrons inside a biofilm. Since the power output from immobilized culture at 150 μmol photons $m^{-2}s^{-1}$ was not affected by the low light harvesting efficiency and electron transport rate of the culture, the high power density in

both the light and dark conditions was thus due to high number of algal cells that were in contact with the ITO-coated anode. This process was highlighted by Angelaalincy *et al.* (2018) when they explained that the most dynamic electrochemical reaction takes place at the lowest deposited layer of cells in a biofilm where closest contact between the cells and the electrode is established. Although electron deposition leads to increased electrochemical activity on the electrode in both light and dark phases, the effect of irradiance on electrogenic activities at the anode was more evident in illuminated conditions with higher power output and voltage under light conditions. In this study, the highest power density and voltage under light conditions were 0.456 ± 0.026 mWm^{-2} and 0.095 V whereas the corresponding power density and voltage after dark adaptation were 0.430 ± 0.126 mWm^{-2} and 0.089 V respectively. These findings are in agreement with the higher voltage and power output in the light phase reported by Pisciotta *et al.* (2010) who found that the weakened positivity of the anode potential due to electron buildup was responsible for a higher voltage in the irradiated culture. According to Ohm's Law and Power Law, power output is directly proportional to voltage squared at fixed resistance. Hence, high voltage from immobilized cultures at 150 µmol photons m^{-2} s^{-1} was tied to high power density from the BPV devices at the same irradiance level. Although the source of electrons in the algal BPV devices was mainly from splitting of water by light energy, power density in dark phase was found to be insignificantly different ($P>0.05$) from power density in light phase. In dark conditions, algal cells are still able to derive energy by consuming organic carbon sources (Morales-Sánchez *et al.*, 2015), as dark respiration provides energy for maintenance and biosynthesis in the absence of light (Perez-Garcia *et al.*, 2011).

When irradiance was increased to 210 µmol photons m^{-2} s^{-1}, there was a 58.8% difference in maximum power density from immobilized cultures between 30 µmol

photons $m^{-2} s^{-1}$ and 210 μmol photons $m^{-2} s^{-1}$, whereby the maximum power density values were 0.250±0.008 mWm^{-2} and 0.103±0.002 mWm^{-2} respectively. The disparity between the power output values initially suggested that the algal cells may have been partially photoinhibited when grown under an irradiance of 210 μmol photons $m^{-2} s^{-1}$. High irradiance level is understood to induce disequilibrium between the rate of photodamage on PS II and the rate of repair of PS II (Murata *et al.*, 2007), resulting in a decrease in electron transport rate followed by a delayed regression of the electron transfer chain to its original state for the next round of electron flow to ensue (Han *et al.*, 2000). In response to high irradiance, hindrance to the water splitting process impedes reduction of the PSII primary electron donor, P_{680}^{+} which then remains in its strong oxidized state and turns the PSII reaction centers into a dysfunctional state (Takahashi & Murata, 2008). In this experiment, the ability of the algal cells to capture light was defined with high light harvesting efficiency readings but the combination of low NPQ and F_v/F_m readings at the same light condition were evidence of algal cells' inability to effectively dissipate excess energy in terms of fluorescence and heat due to partial photoinhibition.

At the same irradiance level of 210 μmol photons $m^{-2} s^{-1}$, protection against photodamage in the suspension culture was more effective than immobilized culture in spite of the apparent effect of photo-induced stress that was exhibited in terms of relatively poor F_v/F_m, $rETR_{max}$, NPQ and α values. The NPQ trend in the suspension culture was unanticipated as upregulation of NPQ along with elevation of violaxanthin de-epoxidation for photoprotection has been widely reported in literature. Nevertheless, discrepancy on the linear correlation between NPQ and xanthophyll regulation was already discussed by Masojídek *et al.* (1999) when zeaxanthin continued to be synthesized throughout illumination period despite NPQ ceasing to increase further after 30 minutes of irradiation. According to Jahns and Holzwarth (2012), ΔpH removal is the

key instrument to NPQ moderation in green algae, thereby the role of zeaxanthin in photoprotection could have been performed by other xanthophyll components (Niyogi *et al.*, 1997), since xanthophylls are not the primary controller of NPQ.

Findings from the present study clearly indicated that immobilized algal cells were able to produce higher power output than suspension cultures. These results were expected as algal cell immobilization within a matrix develops a truncated pathway for efficient electron transfer due to improved cellular contact between amassed cells (Ng *et al.*, 2017). The cross-linkage between G-blocks of alginate and Ca^{2+} ions forms a stable hydrogel environment (Lee & Mooney, 2012), thus constructing a strong platform for mass transfer between the immobilized algae cells and the anode surface. A shorter electron flow distance before electron-electrode contact was attained corresponds with a higher effectiveness in electron transfer (Angelaalincy *et al.*, 2018). The close contact between immobilized cells and the anode surface would enhance interfacial charge transmittance by minimizing charge transfer resistance (Wang *et al.*, 2015). Apart from charge transfer resistance, a slash in internal resistance improves power yield from a photosynthetic fuel cell (Helder *et al.*, 2012). Zhou *et al.* (2012) elaborated that the diminution of the device's internal resistance promotes higher power output when cellular entrapment in alginate prevents deposition of mobilizing algal cells in the suspension culture on the anode surface. The constraining effect of the alginate gel on the algal cells also stimulates manufacturing of photosynthetic pigments when mutual cell shading minimizes light absorption (Abdel Hameed & Ebrahim, 2007). Hu *et al.* (2016) presented results on improved electricity production with increasing irradiance but maximum power and potential yield deteriorated in response to excessive light. Hence, it is evident from this study that enhancement in bioelectricity generation from suspension and immobilized

cultures is subjected to increasing irradiance level until the respective light saturating limit is reached.

5.3 Effect of Different Irradiance Levels on Photosynthetic Performance

5.3.1 Effect on Maximum Quantum Efficiency, F_v/F_m

Suspension cultures in this study had F_v/F_m values that were within the range of 0.510 ± 0.116 and 0.748 ± 0.012. Regular F_v/F_m values for microalgae to thrive are between 0.7 and 0.8 (Malapascua *et al.*, 2014). In the study conducted by Parkhill *et al.* (2001), the threshold F_v/F_m value for algal cells to be considered healthy was around 0.6. At 210 μmol photons m^{-2} s^{-1}, F_v/F_m values of the suspension cultures did not surpass 0.6, thus implying that the algal cells were already under photo-induced stress. Upon illumination with high irradiance, the reduction process of the active binding site Q_A may become dominant over reoxidation of its reduced state, Q_A^- (Rym, 2012). The failure of Q_A^- to return to its stable state upsets the flow of electrons to the plastoquinone in Q_B and subsequently, to the cytochrome b_6f complex and PSI. Once the electron flow along the electron transport chain is disrupted due to high irradiance stress which sets off photoinhibition, reemission of light as fluorescence becomes recessive, explaining the reason for the decrease in F_v/F_m values.

In general, the F_v/F_m values for immobilized cultures began dropping after Day 8, possibly due to nutrient depletion as a result of significant increase in cell density (Ng *et al.*, 2017). Shrinkage in nutrients supply signals the cells to shift from the exponential phase to stationary phase (Fleming, 2010), in which the cells were likely to experience nitrogen deficiency as nutrient uptake would have been higher when the algal cells were actively multiplying during the exponential growth phase. Falkowski *et al.* (1992) provided supporting evidence that nutrient deprivation was a significant factor in diminishing maximum quantum yield of photosynthetic organisms. Nevertheless, biomass continued growing in immobilized cultures at 30 μmol photons m^{-2} s^{-1} in Set 1

and 210 µmol photons m^{-2} s^{-1} on Day 12 due to the alginate gel matrix protecting the algal cells from desiccation which will eventually lead to the death phase.

5.3.2 Effect on Maximum Relative Electron Transport Rate, rETR$_{max}$

The change in irradiance affects maximum relative electron transport rate (rETR$_{max}$) through biophysical changes in the structures of the photosynthetic apparatus of the algae cells. Exposure of algae cells to high irradiance stimulates mutual cell shading as well as shifting of chlorophyll sites, thus affecting the cross-sectional area of PSII involved in light absorptance for photochemistry (Figueroa *et al.*, 2003). The rETR$_{max}$ data in this experiment conform to these concepts but only to a certain extent. The non-linear relationship between different irradiance levels and photosynthetic electron transport was once suggested by Harbinson *et al.* (1990). A similar scenario can be modeled from the results of this study. A plausible explanation for the decrease in electron transport rate at 150 µmol photons m-2 s-1 is the increase in irradiance from 90 µmol photons m-2 s-1 induced lumen acidification which saturates the electron transport pathway and activates the photodamage protection mechanism NPQ (Anderson & Chow, 2002). When excessive light is absorbed by the algal cells, pH drop in the thylakoid lumen sets off energy-dependent quenching, qE and xanthophyll production for photoprotection (Müller *et al*., 2001). There have been numerous reports on the direct relationship between NPQ and changes in carotenoids such as zeaxanthin and anteraxanthin in chloroplasts (Latowski *et al.,* 2011). Discussion by Jahns and Holzwarth (2012) highlighted the intertwining of ΔpH in the thylakoid membrane, zeaxanthin functionality and PsbS activation. PsbS acts as a sensor that responds to transmembrane acidification which then leads to the initiation of violaxanthin de-epoxidation for zeaxanthin synthesis in the xanthophyll cycle (Wilk *et al*., 2013). The high carotenoids readings at 150 µmol photons m-2 s-1 supplement with the rETRmax readings at the same irradiance, thus

concluding that elevated production of xanthophyll at this irradiance level reveals initiation of cellular photoprotection response that limits electron transport by thylakoid lumen acidification (Foyer *et al.*, 2012; Järvi *et al.*, 2013).

5.3.3 Effect on Light Harvesting Efficiency, α

The high α values for BPV devices containing both suspension and immobilized cultures that were exposed to 210 µmol photons $m^{-2} s^{-1}$ of irradiance were expected based on the greater radiant flux received by PSII of the algal cells and high cell concentrations. Theoretically, a high α value should correspond to high power output since the large number of algal cells are able to harvest more light energy for excitation of electrons in PS II but current density and power density at 210 µmol photons $m^{-2} s^{-1}$ did not conform with the corresponding α readings. Here, light harvesting efficiency and light utilizing efficiency are clearly two distinct parameters. Even if the algal cells were able to harvest all the light impinged on the surface of the cells, not all the light were converted into useful energy as the protection mechanism of the algal cells diverted excess energy out of PSII once light began to get saturated in PSII. As mentioned by Iluz *et al.* (2012), utilization of photons by microalgae is only partial despite complete absorption of all the light received. Although the light harvesting efficiency of the algal cells was excellent, high F_v/F_m and NPQ values of immobilized cultures at 210 µmol photons $m^{-2} s^{-1}$ verified that light utilization was rather incomplete with part of the light absorbed eventually dissipated as fluorescence and heat.

5.3.4 Effect on Photoadaptive Index, E_k

Evaluation on the photoadaptive index, E_k data suggests that the algal cells were able to adapt to the irradiance level received until the effects of photoinhibition were revealed in terms of low E_k and NPQ readings. The higher E_k at 90 µmol photons $m^{-2} s^{-1}$

compared to the E_k at 30 μmol photons $m^{-2} s^{-1}$ represents higher cellular ability at 90 μmol photons $m^{-2} s^{-1}$ to acclimatize to the irradiance exposed. This can be attributed to high photosynthetic capacity of the cells as high F_v/F_m values implied that positive physiological state would support the light utilization capacity of the algal cells. In parallel to the high F_v/F_m values, the relatively low NPQ readings were indicative of minimal need for redistribution of excess light energy in the form of heat. Maximum power density generated at 90 μmol photons $m^{-2} s^{-1}$ further confirms adaptation of the algal cells to this irradiance level. While E_k at 90 μmol photons $m^{-2} s^{-1}$ was high, the E_k at 210 μmol photons $m^{-2} s^{-1}$ was significantly lower especially on Days 0, 4 and 8 of the experiment. The noteworthy difference between E_k at 90 μmol photons $m^{-2} s^{-1}$ and 210 μmol photons $m^{-2} s^{-1}$ was suggestive about the response of algal cells to dissimilar irradiance levels. With correspondence to low F_v/F_m, $rETR_{max}$ and maximum power density, initial signs of photoinhibition in the suspension culture at 210 μmol photons $m^{-2} s^{-1}$ were apparent. Low carotenoids readings at 210 μmol photons $m^{-2} s^{-1}$ provided additional verification for the relationship between ineffective photoprotection mechanism and low E_k in the suspension culture.

A similar trend for E_k values in suspension cultures can be observed for E_k values in immobilized cultures but E_k at 150 μmol photons $m^{-2} s^{-1}$ turned out to be lower than E_k at 210 μmol photons $m^{-2} s^{-1}$. The mutual cell shading effect is understood to be the cause of this phenomenon. E_k started off high on Day 0 but it declined significantly on Day 4 and remained relatively constant until Day 12. Sudden restrictions to cell mobility as well as exposure to 150 μmol photons $m^{-2} s^{-1}$ of light drove the algal cells to photoacclimation. During adaptation to ambient light, enlargement of thylakoid area takes place to accommodate increasing amount of chlorophyll content in the algal cells (Dubinsky & Stambler, 2009). Since the algal cells were trapped in the gel matrix, the increase in cell

density promoted mutual cell shading that eventually reduced light harvesting efficiency of the cells (Fisher *et al.*, 1996). Concomitantly, the increase of α from 0.211±0.013 on Day 0 to 0.617±0.013 on Day 4 denoted photoacclimation whereas the decrease to 0.485±0.008 on Day 8 and 0.391±0.009 on Day 12 was resulted from mutual shading.

CHAPTER 6: CONCLUSION

The integration of microalgae into fuel cell technology has so far been promising with apparent benefits in terms of economic, spatial and environmental aspects. Bioelectricity generation from abundant sources of natural living organisms like microalgae does not disrupt the ecosystem balance due to minimal negative effects of the redox system to the environment. In fact, algal BPV platforms contribute to carbon sequestration through carbon dioxide intake for photosynthesis to occur. Although not discussed in this dissertation, there have also been reports of algal BPV devices now serving a secondary purpose, that is, to treat wastewater when algae feed on the nutrients in the wastewater. The many advantages of utilizing algal BPV devices underline the importance of more research activities like this study to comprehend the functionalities of the devices as a dependable clean and renewable energy source.

Previously, suspension algal cultures were commonly used in algal BPV devices for power generation but a reported 18% increase in power output from BPV devices containing alginate-immobilized algal cells as compared to conventional suspension algal cultures by Ng *et al.* (2017) sparked interest to investigate how different irradiance levels influence algal photosynthetic performance and power generation from algal BPV devices of the same design in this research project. Results from the present study clearly shows that immobilized cultures, in general, are able to produce higher power density than suspension cultures. Power output from the algal BPV devices used in this study increased with increasing irradiance level but only to the extent of 150 μmol photons m^{-2} s^{-1} as power output was lowest at 210 μmol photons m^{-2} s^{-1}, thus denoting the occurrence of partial photoinhibition in the algae. The optimum irradiance level that produced maximum power output from suspension cultures was 90 μmol photons m^{-2} s^{-1} but a

higher irradiance level of 150 μmol photons $m^{-2} s^{-1}$ was required for maximum power output from immobilized cultures in these algal BPV devices. In the present study, the highest power output obtained from immobilized cultures was 0.456 ± 0.026 mWm^{-2}. This power output value was 57.79% higher than the 0.289 ± 0.004 mWm^{-2} previously reported by our research group (Ng *et al.*, 2017).

Currently, limitations in terms of magnitude of the power output from algal BPV devices are rendering these platforms as less practical for up-scaled applications, Hence, fundamental studies on the various aspects of algal BPV devices need to be continuous for optimization of an efficient algal BPV system. Although the number of studies on a wide range of essential subjects such as selection of algal species, biomass and effects of physical factors like light, temperature, salinity and pH on algal photosynthetic performance, have been reported, the complex nature of algal physiological responses towards external stimuli requires more in-depth experiments to be conducted. This present study involved the response of *Chlorella* sp. in flat-plate BPV devices towards one factor only, that is different irradiance levels. Further work on other factors like temperature, pH, nutrient levels, etc. as well as the interactive effects of these factors, should be conducted. However, the findings of the present study provide very useful information for future improvements on the existing algal BPV devices used in this research. The several limitations which include light attenuation, mutual cell shading and partial photoinhibition at high irradiance level will be taken into consideration when the design of the algal BPV devices is revised. From the chemistry and physics perspectives, selection of appropriate materials for the anode and cathode imparts huge impact on the performance of BPV platforms. In the near future, the direction of research focus on algal BPV devices should shift to key factors like electrical conductivity of the electrode materials as well as enhanced compatibility of the electrodes with the algal cells.

REFERENCES

Abdel Hameed, M. S., & Ebrahim, O. H. (2007). Review: Biotechnological potential uses of immobilized algae. *International Journal of Agriculture and Biology, 9*(1), 183-192.

Amini Khoeyi, Z., Seyfabadi, J., & Ramezanpour, Z. (2012). Effect of light intensity and photoperiod on biomass and fatty acid composition of the microalgae, *Chlorella vulgaris*. *Aquaculture International, 20*(1), 41-49.

Andersen, R. A. (Ed.). (2005). *Algal culturing techniques*. Burlington, MA: Elsevier Academic Press.

Anderson, J. M., & Chow, W. S. (2002). Structural and functional dynamics of plant photosystem II. *Philosophical Transactions of the Royal Society B: Biological Sciences, 357*(1426), 1421-1470.

Andersson, B., Salter, A. H., Virgin, I., Vass, I., & Styring, S. (1992). Photodamage to photosystem II - Primary and secondary events. *Journal of Photochemistry and Photobiology B: Biology, 15*(1), 15-31.

Angelaalincy, M. J., Navanietha Krishnaraj, R., Shakambari, G., Ashokkumar, B., Kathiresan, S., & Varalakshmi, P. (2018). Biofilm engineering approaches for improving the performance of microbial fuel cells and bioelectrochemical systems. *Frontiers in Energy Research, 6*, 63.

Apel, K., & Hirt, H. (2004). Reactive oxygen species: Metabolism, oxidative stress, and signal transduction. *Annual Review of Plant Biology, 55*(1), 373-399.

Aro, E.-M., Virgin, I., & Andersson, B. (1993). Photoinhibition of photosystem II. Inactivation, protein damage and turnover. *Biochimica et Biophysica Acta (BBA) - Bioenergetics, 1143*(2), 113-134.

Barber, J. (2009). Photosynthetic energy conversion: Natural and artificial. *Chemical Society Reviews, 38*(1), 185-196.

Bard, A. J., & Fox, M. A. (1995). Artificial photosynthesis: Solar splitting of water to hydrogen and oxygen. *Accounts of Chemical Research, 28*(3), 141-145.

Bayramoğlu, G., Tuzun, I., Celik, G., Yilmaz, M., & Arica, M. Y. (2006). Biosorption of mercury(II), cadmium(II) and lead(II) ions from aqueous system by microalgae *Chlamydomonas reinhardtii* immobilized in alginate beads. *International Journal of Mineral Processing, 81*(1), 35-43.

Bombelli, P., Müller, T., Herling Therese, W., Howe Christopher, J., & Knowles Tuomas, P. J. (2014). A high power-density, mediator-free, microfluidic biophotovoltaic device for cyanobacterial cells. *Advanced Energy Materials, 5*(2), 1401299.

Bombelli, P., Zarrouati, M., Thorne, R. J., Schneider, K., Rowden, S. J. L., Ali, A., . . . McCormick, A. J. (2012). Surface morphology and surface energy of anode materials influence power outputs in a multi-channel mediatorless bio-photovoltaic (BPV) system. *Physical Chemistry Chemical Physics, 14*(35), 12221-12229.

Bosire, E. M., & Rosenbaum, M. A. (2017). Electrochemical potential influences phenazine production, electron transfer and consequently electric current generation by *Pseudomonas aeruginosa*. *Frontiers in Microbiology, 8*.

Brotosudarmo, T. H. P., Prihastyanti, M. N. U., Gardiner, A. T., Carey, A.-M., & Cogdell, R. J. (2014). The light reactions of photosynthesis as a paradigm for solar fuel production. *Energy Procedia, 47*, 283-289.

Carmona-Martínez, A. A., Harnisch, F., Kuhlicke, U., Neu, T. R., & Schröder, U. (2013). Electron transfer and biofilm formation of *Shewanella putrefaciens* as function of anode potential. *Bioelectrochemistry, 93*, 23-29.

Carvalho, A. P., Silva, S. O., Baptista, J. M., & Malcata, F. X. (2011). Light requirements in microalgal photobioreactors: An overview of biophotonic aspects. *Applied Microbiology and Biotechnology, 89*(5), 1275-1288.

Choudhury, A., Barbora, L., Arya, D., Lal, B., Subudhi, S., Mohan, S. V., . . . Verma, A. (2016). Effect of electrode surface properties on enhanced electron transfer activity in microbial fuel cells. *Engineering in Life Sciences, 17*(2), 186-192.

Ciniciato, G. P. M. K., Ng, F.-L., Phang, S.-M., Jaafar, M. M., Fisher, A. C., Yunus, K., & Periasamy, V. (2016). Investigating the association between photosynthetic efficiency and generation of biophotoelectricity in autotrophic microbial fuel cells. *6*, 31193.

Das, M., & Adholeya, A. (2015). Potential uses of immobilized bacteria, fungi, algae, and their aggregates for treatment of organic and inorganic pollutants in wastewater. In *Water challenges and solutions on a global scale* (Vol. 1206, pp. 319-337): American Chemical Society.

de-Bashan, L. E., & Bashan, Y. (2010). Immobilized microalgae for removing pollutants: Review of practical aspects. *Bioresource Technology, 101*(6), 1611-1627.

Demmig-Adams, B., & Adams, W. W. III (1996). The role of xanthophyll cycle carotenoids in the protection of photosynthesis. *Trends in Plant Science, 1*(1), 21-26.

Demmig-Adams, B., & Adams, W.W. III. (2003). Photoprotection and other responses of plants to high light stress. *Annual Review of Plant Physiology and Plant Molecular Biology, 43,* 599-626.

Devrimci, H. A., Yuksel, A. M., & Sanin, F. D. (2012). Algal alginate: A potential coagulant for drinking water treatment. *Desalination, 299,* 16-21.

Dubinsky, Z., & Stambler, N. (2009). Photoacclimation processes in phytoplankton: Mechanisms, consequences, and applications. *Aquatic Microbial Ecology*, *56*(2), 163-176.

Ertesvåg, H., & Valla, S. (1998). Biosynthesis and applications of alginates. *Polymer Degradation and Stability, 59*(1), 85-91.

Falkowski, P. G., Greene, R. M., & Geider, R., J. . (1992). Physiological limitations on phytoplankton productivity in the ocean. *Oceanography, 5*(2), 84-91.

Fiedor, J., & Burda, K. (2018). Carotenoids—Antioxidant properties. *Antioxidants, 7*(2), 28.

Figueroa, F. L., Conde-Álvarez, R., & Gómez, I. (2003). Relations between electron transport rates determined by pulse amplitude modulated chlorophyll fluorescence and oxygen evolution in macroalgae under different light conditions. *Photosynthesis Research, 75*(3), 259-275.

Fischer, F. (2018). Photoelectrode, photovoltaic and photosynthetic microbial fuel cells. *Renewable and Sustainable Energy Reviews, 90,* 16-27.

Fisher, T., Minnaard, J., & Dubinsky, Z. (1996). Photoacclimation in the marine alga *Nannochloropsis* sp. (Eustigmatophyte): A kinetic study. *Journal of Plankton Research*, *18*(10), 1797-1818. w

Fleming, J. T. (2010). Electronic interfacing with living cells. In S. Belkin, & M. B. Gu, Eds.), *Whole cell sensing systems I: Reporter cells and devices* (pp. 155-178). Heidelberg, Germany: Springer.

Foyer, C. H., Neukermans, J., Queval, G., Noctor, G., & Harbinson, J. (2012). Photosynthetic control of electron transport and the regulation of gene expression. *Journal of Experimental Botany, 63*(4), 1637-1661.

Freire, R. S., Pessoa, C. A., Mello, L. D., & Kubota, L. T. (2003). Direct electron transfer: An approach for electrochemical biosensors with higher selectivity and sensitivity. *Journal of the Brazilian Chemical Society, 14*(2), 230-243.

Gatamaneni, B. L., Orsat, V., & Lefstrud, M. (2018). Factors affecting growth of various microalgal species. *Environmental Engineering Science, 35*(10), 1037-1048.

Genty, B., Briantais, J.-M., & Baker, N. R. (1989). The relationship between the quantum yield of photosynthetic electron transport and quenching of chlorophyll fluorescence. *Biochimica et Biophysica Acta (BBA) - General Subjects, 990*(1), 87-92.

Guedes, A. C., Meireles, L. A., Amaro, H. M., & Malcata, F. X. (2010). Changes in lipid class and fatty acid composition of cultures of *Pavlova lutheri*, in response to light intensity. *Journal of the American Oil Chemists' Society, 87*(7), 791-801.

Guisan, J. M. (2006). *Immobilization of enzymes and cells* (2nd ed.). Totowa, N.J.: Humana Press.

Guo, K. (2014). *The effects of electrode surface modifications on biofilm formation and electron transfer in bioelectrochemical systems.* (Doctor of Philosophy; Doctor of Applied Biological Sciences), University of Queensland; Ghent University, Brisbane St Lucia, QLD, Australia ; Ghent, Belgium. (4392628)

Han, B.-P., Virtanen, M., Koponen, J., & Straškraba, M. (2000). Effect of photoinhibition on algal photosynthesis: A dynamic model. *Journal of Plankton Research, 22*(5), 865-885.

Harbinson, J., Genty, B., & Baker, N. R. (1990). The relationship between CO_2 assimilation and electron transport in leaves. *Photosynthesis Research, 25*(3), 213-224.

Helder, M., Strik, D. P., Hamelers, H. V. M., & Buisman, C. J. N. (2012). The flat-plate plant-microbial fuel cell: The effect of a new design on internal resistances. *Biotechnology for Biofuels, 5*(1), 70.

Hu, Q., & Richmond, A. (1996). Productivity and photosynthetic efficiency of *Spirulina platensis* as affected by light intensity, algal density and rate of mixing in a flat plate photobioreactor. *Journal of Applied Phycology, 8*(2), 139-145.

Hu, X., Zhou, J., & Liu, B. (2016). Effect of algal species and light intensity on the performance of an air-lift-type microbial carbon capture cell with an algae-assisted cathode. *RSC Advances, 6*(30), 25094-25100.

Iluz, D., Irit, & Dubinsky, Z. (2012). The enhancement of photosynthesis by fluctuating light. In M. Najafpour (Ed.), *Artificial Photosynthesis*. Retrieved 20 July 2018, from https://www.intechopen.com/books/artificial-photosynthesis/the-enhancement-of-photosynthesis-by-fluctuating-light.

Jahns, P., & Holzwarth, A. R. (2012). The role of the xanthophyll cycle and of lutein in photoprotection of photosystem II. *Biochimica et Biophysica Acta (BBA) - Bioenergetics, 1817*(1), 182-193.

Järvi, S., Gollan, P. J., & Aro, E.-M. (2013). Understanding the roles of the thylakoid lumen in photosynthesis regulation. *Frontiers in Plant Science, 4*, 434.

Johnson, Matthew P. (2016). Photosynthesis. *Essays in Biochemistry, 60*(3), 255-273.

Kato, M. C., Hikosaka, K., Hirotsu, N., Makino, A., & Hirose, T. (2003). The excess light energy that is neither utilized in photosynthesis nor dissipated by photoprotective mechanisms determines the rate of photoinactivation in photosystem II. *Plant and Cell Physiology, 44*(3), 318-325.

Kim, H. S., Lee, C.-G., & Lee, E. Y. (2011). Alginate lyase: Structure, property, and application. *Biotechnology and Bioprocess Engineering, 16*(5), 843.

Kosourov, S. N., & Seibert, M. (2008). Hydrogen photoproduction by nutrient-deprived *Chlamydomonas reinhardtii* cells immobilized within thin alginate films under aerobic and anaerobic conditions. *Biotechnology and Bioengineering, 102*(1), 50-58.

Krause, G. H. (1988). Photoinhibition of photosynthesis. An evaluation of damaging and protective mechanisms. *Physiologia Plantarum, 74*(3), 566-574.

Krause, G. H., Vernotte, C., & Briantais, J. M. (1982). Photoinduced quenching of chlorophyll fluorescence in intact chloroplasts and algae. Resolution into two components. *Biochimica et Biophysica Acta (BBA) - Bioenergetics, 679*(1), 116-124.

Krieger-Liszkay, A., Fufezan, C., & Trebst, A. (2008). Singlet oxygen production in photosystem II and related protection mechanism. *Photosynthesis Research, 98*(1), 551-564.

Ksas, B., Becuwe, N., Chevalier, A., & Havaux, M. (2015). Plant tolerance to excess light energy and photooxidative damage relies on plastoquinone biosynthesis. *Scientific Reports, 5*, 10919.

Lambrev, P. H., Miloslavina, Y., Jahns, P., & Holzwarth, A. R. (2012). On the relationship between non-photochemical quenching and photoprotection of photosystem II. *Biochimica et Biophysica Acta (BBA) - Bioenergetics, 1817*(5), 760-769.

Laohavisit, A., Anderson, A., Bombelli, P., Jacobs, M., Howe, C. J., Davies, J. M., & Smith, A. G. (2015). Enhancing plasma membrane NADPH oxidase activity increases current output by diatoms in biophotovoltaic devices. *Algal Research, 12*, 91-98.

Latifi, A., Ruiz, M., & Zhang, C.-C. (2009). Oxidative stress in cyanobacteria. *FEMS Microbiology Reviews, 33*(2), 258-278.

Latowski, D., Kuczyńska, P., & Strzałka, K. (2011). Xanthophyll cycle – A mechanism protecting plants against oxidative stress. *Redox Report, 16*(2), 78-90.

Lee, K. Y., & Mooney, D. J. (2012). Alginate: Properties and biomedical applications. *Progress in Polymer Science, 37*(1), 106-126.

Lewis, N. S., & Nocera, D. G. (2006). Powering the planet: Chemical challenges in solar energy utilization. *Proceedings of the National Academy of Sciences, 103*(43), 15729.

Li, J., Zhao, Y., Wang, N., Ding, Y., & Guan, L. (2012). Enhanced performance of a MnO_2–graphene sheet cathode for lithium ion batteries using sodium alginate as a binder. *Journal of Materials Chemistry, 22*(26), 13002-13004.

Liu, Y., Daye, J., Jenson, D., & Fong, S. (2018). Evaluating the efficiency of a photoelectrochemical electrode constructed with photosystem II-enriched thylakoid membrane fragments. *Bioelectrochemistry, 124*, 22-27.

Mahmoudzadeh, A., Saer, R., Jun, D., Mirvakili, S. M., Takshi, A., Iranpour, B., . . . Beatty, J. T. (2011). Photocurrent generation by direct electron transfer using photosynthetic reaction centres. *Smart Materials & Structures, 20*(9). 094019.

Malapascua, J. R. F., Jerez, C. G., Sergejevová, M., Figueroa, F. L., & Masojídek, J. (2014). Photosynthesis monitoring to optimize growth of microalgal mass cultures: Application of chlorophyll fluorescence techniques. *Aquatic Biology, 22*, 123-140.

Mallick, N., & Mohn, F. H. (2000). Reactive oxygen species: Response of algal cells. *Journal of Plant Physiology, 157*(2), 183-193.

Mao, L., & Verwoerd, W. S. (2013). Selection of organisms for systems biology study of microbial electricity generation: A review. *International Journal of Energy and Environmental Engineering, 4*(1), 17.

Martinsen, A., Skjåk-Bræk, G., & Smidsrød, O. (1989). Alginate as immobilization material: I. Correlation between chemical and physical properties of alginate gel beads. *Biotechnology and Bioengineering, 33*(1), 79-89.

Masojídek, J., Torzillo, G., & Koblížek, M. (2013). Photosynthesis in microalgae. In A. Richmond & Q. Hu (Eds.), *Handbook of Microalgal Culture*. (pp. 21-36). Hoboken, NJ: Wiley-Blackwell.

Masojídek, J., Torzillo, G., Koblížek, M., Kopecký, J., Bernardini, P., Sacchi, A., & Komenda, J. (1999). Photoadaptation of two members of the Chlorophyta (*Scenedesmus* and *Chlorella*) in laboratory and outdoor cultures: Changes in chlorophyll fluorescence quenching and the xanthophyll cycle. *Planta, 209*(1), 126-135.

Maxwell, K., & Johnson, G. N. (2000). Chlorophyll fluorescence—A practical guide. *Journal of Experimental Botany, 51*(345), 659-668.

McCormick, A. J., Bombelli, P., Scott, A. M., Philips, A. J., Smith, A. G., Fisher, A. C., & Howe, C. J. (2011). Photosynthetic biofilms in pure culture harness solar energy in a mediatorless bio-photovoltaic cell (BPV) system. *Energy & Environmental Science, 4*(11), 4699-4709.

McEvoy, J. P., Gascon, J. A., Batista, V. S., & Brudvig, G. W. (2005). The mechanism of photosynthetic water splitting. *Photochemical & Photobiological Sciences, 4*(12), 940-949.

Mettler, T., Mühlhaus, T., Hemme, D., Schöttler, M.-A., Rupprecht, J., Idoine, A., . . . Stitt, M. (2014). Systems analysis of the response of photosynthesis, metabolism, and growth to an increase in irradiance in the photosynthetic model organism *Chlamydomonas reinhardtii*. *The Plant Cell, 26*(6), 2310.

Mitra, M., & Melis, A. (2008). Optical properties of microalgae for enhanced biofuels production. *Optics Express, 16*(26), 21807-21820.

Mohan, S. V., & Devi, M. P. (2014). Salinity stress induced lipid synthesis to harness biodiesel during dual mode cultivation of mixotrophic microalgae. *Bioresource Technology, 165*, 288-294.

Morales-Sánchez, D., Martinez-Rodriguez, O. A., Kyndt, J., & Martinez, A. (2015). Heterotrophic growth of microalgae: Metabolic aspects. *World Journal of Microbiology and Biotechnology, 31*(1), 1-9.

Moreira, S. M., Moreira-Santos, M., Guilhermino, L., & Ribeiro, R. (2006). Immobilization of the marine microalga *Phaeodactylum tricornutum* in alginate for in situ experiments: Bead stability and suitability. *Enzyme and Microbial Technology, 38*(1), 135-141.

Müller, P., Li, X., & Niyogi, K. K. (2001). Non-photochemical quenching. A response to excess light energy. *Plant Physiology, 125*(4), 1558-1566.

Murata, N., Allakhverdiev, S. I., & Nishiyama, Y. (2012). The mechanism of photoinhibition in vivo: Re-evaluation of the roles of catalase, α-tocopherol, non-photochemical quenching, and electron transport. *Biochimica et Biophysica Acta (BBA) - Bioenergetics, 1817*(8), 1127-1133.

Murata, N., Takahashi, S., Nishiyama, Y., & Allakhverdiev, S. I. (2007). Photoinhibition of photosystem II under environmental stress. *Biochimica et Biophysica Acta (BBA) - Bioenergetics, 1767*(6), 414-421.

Murray, J. W., & Barber, J. (2007). Structural characteristics of channels and pathways in photosystem II including the identification of an oxygen channel. *Journal of Structural Biology, 159*(2), 228-237.

Neidhardt, J., Benemann, J. R., Zhang, L., & Melis, A. (1998). Photosystem-II repair and chloroplast recovery from irradiance stress: Relationship between chronic photoinhibition, light-harvesting chlorophyll antenna size and photosynthetic productivity in *Dunaliella salina* (green algae). *Photosynthesis Research, 56*(2), 175-184.

Ng, F.-L., Jaafar, M. M., Phang, S.-M., Chan, Z., Salleh, N. A., Azmi, S. Z., . . . Periasamy, V. (2014a). Reduced graphene oxide anodes for potential application in algae biophotovoltaic platforms. *Scientific Reports, 4*, 7562.

Ng, F.-L., Phang, S.-M., Periasamy, V., Yunus, K., & Fisher, A. C. (2014b). Evaluation of algal biofilms on indium tin oxide (ITO) for use in biophotovoltaic platforms based on photosynthetic performance. *PLoS ONE, 9*(5), e97643.

Ng, F.-L., Phang, S.-M., Periasamy, V., Yunus, K., & Fisher, A. C. (2017). Enhancement of power output by using alginate immobilized algae in biophotovoltaic devices. *7*(1), 16237.

Nichols, H. W., & Bold, H. C. (1965). *Trichosarcina polymorpha* gen. et sp. nov. *Journal of Phycology, 1*(1), 34-38.

Nilkens, M., Kress, E., Lambrev, P., Miloslavina, Y., Müller, M., Holzwarth, A. R., & Jahns, P. (2010). Identification of a slowly inducible zeaxanthin-dependent component of non-photochemical quenching of chlorophyll fluorescence generated under steady-state conditions in *Arabidopsis*. *Biochimica et Biophysica Acta (BBA) - Bioenergetics, 1797*(4), 466-475.

Nishio, K., Hashimoto, K., & Watanabe, K. (2010). Light/electricity conversion by a self-organized photosynthetic biofilm in a single-chamber reactor. *Applied Microbiology and Biotechnology, 86*(3), 957-964.

Nishiyama, Y., Allakhverdiev, S. I., Yamamoto, H., Hayashi, H., & Murata, N. (2004). Singlet oxygen inhibits the repair of photosystem II by suppressing the translation elongation of the D1 protein in *Synechocystis* sp. PCC 6803. *Biochemistry, 43*(35), 11321-11330.

Niyogi, K. K., Bjorkman, O., & Grossman, A. R. (1997). *Chlamydomonas* xanthophyll cycle mutants identified by video imaging of chlorophyll fluorescence quenching. *The Plant Cell, 9*(8), 1369.

Pannier, A., Soltmann, U., Soltmann, B., Altenburger, R., & Schmitt-Jansen, M. (2014). Alginate/silica hybrid materials for immobilization of green microalgae *Chlorella vulgaris* for cell-based sensor arrays. *Journal of Materials Chemistry B, 2*(45), 7896-7909.

Parkhill, J.-P., Maillet, G., & Cullen John, J. (2001). Fluorescence-based maximal quantum yield for PSII as a diagnostic of nutrient stress. *Journal of Phycology, 37*(4), 517-529.

Pathak, T. S., Kim, J. S., Lee, S.-J., Baek, D.-J., & Paeng, K.-J. (2008). Preparation of alginic acid and metal alginate from algae and their comparative study. *Journal of Polymers and the Environment, 16*(3), 198-204.

Pawar, S. N., & Edgar, K. J. (2012). Alginate derivatization: A review of chemistry, properties and applications. *Biomaterials, 33*(11), 3279-3305.

Perez-Garcia, O., Escalante, F. M. E., de-Bashan, L. E., & Bashan, Y. (2011). Heterotrophic cultures of microalgae: Metabolism and potential products. *Water Research, 45*(1), 11-36.

Pinhassi, R. I., Kallmann, D., Saper, G., Dotan, H., Linkov, A., Kay, A., . . . Rothschild, A. (2016). Hybrid bio-photo-electro-chemical cells for solar water splitting. *Nature Communications, 7*.

Pisciotta, J. M., Zou, Y., & Baskakov, I. V. (2010). Light-dependent electrogenic activity of cyanobacteria. *PLoS ONE, 5*(5), e10821.

Pisciotta, J. M., Zou, Y., & Baskakov, I. V. (2011). Role of the photosynthetic electron transfer chain in electrogenic activity of cyanobacteria. *Applied Microbiology and Biotechnology, 91*(2), 377-385.

Qiao, Y., Bao, S.-J., & Li, C. M. (2010). Electrocatalysis in microbial fuel cells from electrode material to direct electrochemistry. *Energy & Environmental Science, 3*(5), 544-553.

Quaas, T., Berteotti, S., Ballottari, M., Flieger, K., Bassi, R., Wilhelm, C., & Goss, R. (2015). Non-photochemical quenching and xanthophyll cycle activities in six green algal species suggest mechanistic differences in the process of excess energy dissipation. *Journal of Plant Physiology, 172*, 92-103.

Rai, M. P., Gautom, T., & Sharma, N. (2015). Effect of salinity , pH , light intensity on growth and lipid production of microalgae for bioenergy application. *OnLine Journal of Biological Sciences, 15*(4), 260-267.

Ras, M., Steyer, J.-P., & Bernard, O. (2013). Temperature effect on microalgae: A crucial factor for outdoor production. *Reviews in Environmental Science and Bio/Technology, 12*(2), 153-164.

Roach, T., & Krieger-Liszkay, A. K. (2014). Regulation of photosynthetic electron transport and photoinhibition. *Current Protein & Peptide Science, 15*(4), 351–362.

Rochaix, J.-D. (2011). Regulation of photosynthetic electron transport. *Biochimica et Biophysica Acta (BBA) - Bioenergetics, 1807*(3), 375-383.

Rögner, M., Boekema, E. J., & Barber, J. (1996). How does photosystem 2 split water? The structural basis of efficient energy conversion. *Trends in Biochemical Sciences, 21*(2), 44-49.

Rosenbaum, M., He, Z., & Angenent, L. T. (2010). Light energy to bioelectricity: Photosynthetic microbial fuel cells. *Current Opinion in Biotechnology, 21*(3), 259-264.

Saar, K. L., Bombelli, P., Lea-Smith, D. J., Call, T., Aro, E.-M., Müller, T., . . . Knowles, T. P. J. (2018). Enhancing power density of biophotovoltaics by decoupling storage and power delivery. *Nature Energy, 3*(1), 75-81.

Saper, G., Kallmann, D., Conzuelo, F., Zhao, F., Tóth, T. N., Liveanu, V., . . . Adir, N. (2018). Live cyanobacteria produce photocurrent and hydrogen using both the respiratory and photosynthetic systems. *Nature Communications, 9*(1), 2168.

Schmid, T., Messmer, A., Yeo, B.-S., Zhang, W., & Zenobi, R. (2008). Towards chemical analysis of nanostructures in biofilms II: Tip-enhanced Raman spectroscopy of alginates. *Analytical and Bioanalytical Chemistry, 391*(5), 1907-1916.

Schneider, K., Thorne, R. J., & Cameron, P. J. (2016). An investigation of anode and cathode materials in photomicrobial fuel cells. *Philosophical Transactions of the Royal Society A: Mathematical, Physical and Engineering Sciences, 374*(2061).

Schwartz, W. (2007). *Handbook of Phycological Methods, Culture Methods and Growth Measurements.* (J. R. Stein, Ed.): Cambridge, England: Cambridge University Press.

Singh, V. K., Ravi, S. K., Ho, J. W., Wong, J. K. C., Jones, M. R., & Tan, S. C. (2017). Biohybrid Photoprotein-Semiconductor Cells with Deep-Lying Redox Shuttles Achieve a 0.7 V Photovoltage. *Advanced Functional Materials*, 1703689.

Singh, S. P., & Singh, P. (2015). Effect of temperature and light on the growth of algae species: A review. *Renewable and Sustainable Energy Reviews, 50*, 431-444.

Smith, B. M., Morrissey, P. J., Guenther, J. E., Nemson, J. A., Harrison, M. A., Allen, J. F., & Melis, A. (1990). Response of the photosynthetic apparatus in *Dunaliella salina* (green algae) to irradiance stress. *Plant Physiology, 93*(4), 1433-1440.

Strickland, J. D. H., & Parsons, T. R. (1972). *A Practical Handbook of Seawater Analysis* (2nd ed.). Ottawa, Canada: Fisheries Research Board of Canada.

Styring, S., Virgin, I., Ehrenberg, A., & Andersson, B. (1990). Strong light photoinhibition of electrontransport in Photosystem II. Impairment of the function of the first quinone acceptor, Q_A. *Biochimica et Biophysica Acta (BBA) - Bioenergetics, 1015*(2), 269-278.

Takahashi, S., & Badger, M. R. (2011). Photoprotection in plants: A new light on photosystem II damage. *Trends in Plant Science, 16*(1), 53-60.

Takahashi, S., & Murata, N. (2008). How do environmental stresses accelerate photoinhibition? *Trends in Plant Science, 13*(4), 178-182.

Torres, C. I., Marcus, A. K., Lee, H. S., Parameswaran, P., Krajmalnik-Brown, R., & Rittmann, B. E. (2010). A kinetic perspective on extracellular electron transfer by anode-respiring bacteria. *Fems Microbiology Reviews, 34*(1), 3-17.

Trebst, A., Depka, B., & Holländer-Czytko, H. (2002). A specific role for tocopherol and of chemical singlet oxygen quenchers in the maintenance of photosystem II structure and function in *Chlamydomonas reinhardtii*. *FEBS Letters, 516*(1), 156-160.

Van Eerden, F. J., Melo, M. N., Frederix, P. W. J. M., Periole, X., & Marrink, S. J. (2017). Exchange pathways of plastoquinone and plastoquinol in the photosystem II complex. *Nature Communications, 8*.

Wang, W., Wang, Z., Zhu, Q., Han, G., Ding, C., Chen, J., . . . Li, C. (2015). Direct electron transfer from photosystem II to hematite in a hybrid photoelectrochemical cell. *Chemical Communications, 51*(95), 16952-16955.

Xu, C. (2015). *Algae grown anode microbial fuel cell and its application in power generation and biosensor.* (Master of Philosophy Open Access Theses and Dissertations), Hong Kong Baptist University, Hong Kong.

Yabur, R., Bashan, Y., & Hernández-Carmona, G. (2007). Alginate from the macroalgae *Sargassum sinicola* as a novel source for microbial immobilization material in wastewater treatment and plant growth promotion. *Journal of Applied Phycology, 19*(1), 43-53.

Yong, X.-Y., Shi, D.-Y., Chen, Y.-L., Jiao, F., Lin, X., Zhou, J., . . . Zheng, T. (2014). Enhancement of bioelectricity generation by manipulation of the electron shuttles synthesis pathway in microbial fuel cells. *Bioresource Technology, 152*, 220-224.

Young, E., & Beardall, J. (2003). Photosynthetic function *in Dunaliella tertiolecta* (Chlorophyta) during a nitrogen starvation and recovery cycle. *Journal of Phycology*, *39*(5), 897-905.

Zhou, M., He, H., Jin, T., & Wang, H. (2012). Power generation enhancement in novel microbial carbon capture cells with immobilized *Chlorella vulgaris*. *Journal of Power Sources, 214*, 216-219.

Zhu, Y., & Yang, S.-T. (2007). Immobilized cell fermentation for production of chemicals and fuels. In *Bioprocessing for Value-Added Products from Renewable Resources* (pp. 373-396). Amsterdam: Elsevier.

Zou, Y., Pisciotta, J., R. Blake Billmyre, R. B., & Baskakov, I. V. (2009). Photosynthetic microbial fuel cells with positive light response. *Biotechnology and Bioengineering, 104*(5), 939-946.